Available online at www.sciencedirect.com
ScienceDirect
Lithos 92 (2006) 198–221
LITHOS
www.elsevier.com/locate/lithos

Postmagmatic sulphur loss in the Skaergaard Intrusion: Implications for the formation of the Platinova Reef

Jens C.Ø. Andersen *

Camborne School of Mines, School of Geography, Archaeology and Earth Resources, University of Exeter, Tremough Campus, Penryn, Cornwall, TR10 9EZ, United Kingdom

Received 12 January 2005; accepted 27 March 2006
Available online 22 May 2006

Abstract

The stratabound Platinova Au–Pd Reef in the Skaergaard Intrusion is intimately linked to Cu–Fe sulphide minerals and occurs at a level that shows changes in the sulphur concentration and the Cu/S ratio. These features suggest that the reef is related to silicate–sulphide liquid immiscibility in the Skaergaard magma. However, although the evidence is strong, present day sulphur concentrations are too low to support such a model.

The detailed knowledge of the shape, volume, and compositional relations of the Skaergaard lithologies allows for numerical modeling of sulphur and copper concentrations during fractionation of the magma. These data can be evaluated with the current models for sulphur saturation in iron-rich mafic magmas to assess the original sulphur concentrations, the extent of fractionation, the composition of sulphide liquids, and the extent of postmagmatic sulphur loss.

Mass balance modeling yields initial copper and sulphur concentrations of 250 and 894 ppm for the parental magma to the Lower Zone a. Prior to sulphur saturation, Cu behaves as an incompatible element with a bulk partition coefficient in the cumulus material, $D^{Cu}_{cumulus}$ of 0.13 indicating some incorporation of Cu into mafic silicates (probably augite). Sulphur can be assumed to be perfectly incompatible in the cumulus minerals, although it will be included as a component of the interstitial liquid. These values yield sulphur saturation at around 635 ppm Cu and 2607 ppm S. Assuming the sulphur to originally be present as a mixture of monosulphide (MSS) and intermediate solid–solution sulphide (ISS), the primary sulphides in the cumulates would amount to 0.07 modal % through Lower and Middle Zones and 0.53 modal % on average through Upper Zone. The expected weight proportion of primary chalcopyrite/pyrrhotite evolves from 30:70 at the base of LZa through 26:74 at the level of the Platinova Reef to 18:82 at the Sandwich Horizon.

The present-day bornite–magnetite mineral assemblage is likely to have been derived from a primary pyrrhotite–chalcopyrite assemblage through reequilibration and postmagmatic oxidation. Significant sulphur appears to have been lost from the lower and middle parts of the Layered Series (Lower Zone a to Upper Zone b), whereas the sulphides of the Upper Zone c can be explained in the context of a sulphur gain. Local-scale reequilibration of Cu from mafic silicates into sulphides may have contributed to the sulphide mineralogy of the Lower and Middle Zones.

The structure of the Platinova Reef probably formed from an original single, stratabound reef. Sulphur loss through oxidation in upward migrating deuteric or hydrothermal fluids could have caused dissolution and reprecipitation of Pd and Au in a cumulate

* Tel.: +44 1326 371836; fax: +44 1326 371859.
E-mail address: J.C.Andersen@exeter.ac.uk.

doi:10.1016/j.lithos.2006.03.033

with several stratiform redox barriers. This process can thus explain the successive Pd peaks of the reef as well as the variable stratigraphic offset of Pd and Au across the intrusion.

Keywords: Skaergaard Intrusion; Platinova Reef; Gold; Platinum-group elements; Sulphur saturation; Silicate–sulphide liquid immiscibility

1. Introduction

Noble metal occurrences in layered intrusions are commonly intimately associated with sulphide minerals. This is prominently evident from the Merensky Reef of the Bushveld Complex, South Africa, and the Main Sulphide Zone of the Great Dyke of Zimbabwe. It is clear that the formation of sulphides remains one of the most critical processes in the formation of orthomagmatic ore deposits. This appears to be equally true for the Skaergaard Intrusion, where the Platinova Pd–Au Reef (Bird et al., 1991; Andersen et al., 1998; Nielsen, 2001) is intimately associated with sulphide minerals. In Skaergaard, this adds new significance to the distribution and composition of sulphide minerals – bringing one of the enigmas of the intrusion into focus; namely the unusually Cu-rich, Fe-poor sulphide mineral assemblage of the Skaergaard lithologies. This study aims at exploring the fractionation of sulphur and related elements in the Skaergaard magma by numerical modeling to further constrain the formation of the Platinova Reef. Furthermore, as sulphide minerals are locally abundant near the borders of the intrusion, some considerations on the potential influence of contamination have been included. This is of relevance because the Pt/Pd/Au ratios underwent significant fractionation within the intrusion prior to the formation of the reef. Throughout this paper, the notations "sulphur solubility" and "sulphur saturation" refer to silicate–sulphide liquid immiscibility.

2. General geology

The Skaergaard Intrusion is a 3500-m-thick tholeiitic layered intrusion occupying an area of approximately 7×11 km^2 at the mouth of the Kangerlussuaq Fjord, East Greenland (Fig. 1). The intrusion formed 55 Ma ago (Brooks and Gleadow, 1977; Hirschmann et al., 1997) from an evolved, Fe- and Ti-rich tholeiitic parental magma undergoing fractional crystallisation in a closed system (Wager and Deer, 1939; Wager and Brown, 1968). It was emplaced at the unconformity between the Archean basement, a thin succession of Cretaceous and Palaeogene sediments, and a thick succession of Palaeogene picrites and tholeiitic flood basalts. The shape of the intrusion (Fig. 2) appears to be partially controlled by faults (steep margins), partially by host-rock strata (roof and base) allowing it to be approximated by a simple polygonal geometry (Nielsen, 2004). After emplacement and crystallisation, the intrusion was tilted approximately 20° towards the south and eroded to expose an almost complete stratigraphic section.

The intrusion crystallised into three structurally and compositionally distinct lithological units: the Marginal Border Series (MBS) along the walls, the Layered Series (LS) on the floor, and the Upper Border Series (UBS) below the roof of the magma chamber. Each series shows a distinct differentiation trend towards lower temperature mineral assemblages and compositions towards the centre of the intrusion. The magmatic evolution is most clearly expressed in the LS (Fig. 3), where the most primitive exposed unit, Lower Zone a (LZa) is composed of plagioclase–olivine cumulates, augite joins in Lower Zone b (LZb) and titanomagnetite in Lower Zone c (LZc). The onset of ilmenite crystallisation is somewhat obscure, partly because it is masked by the abundant oxyexolved grains of primary titanomagnetite (cf., Buddington and Lindsley, 1964). Wager and Brown (1968) noted the sporadic occurrence of euhedral ilmenite grains in LZb, and certainly, such grains are abundant in LZc. The base of Middle Zone (MZ) is marked by the peritectic replacement of olivine by pigeonite (now inverted to orthopyroxene). Continued evolution towards a lower Mg/Fe ratio caused this reaction to revert in Upper Zone a (UZa), where olivine again appears as a cumulus phase. Apatite joins the fractionating assemblage in Upper Zone b (UZb), and ferrobustamite in Upper Zone c (UZc). The LS and UBS meet at the Sandwich Horizon (SH), which represents the most differentiated part of the intrusion. An unexposed Hidden Zone (HZ) of uncertain thickness and composition underlies the LZa but has not been considered here.

Although the primary lithological units show compositional differences, fractionation trends are roughly parallel in each series. Noticeable differences are higher concentrations of the late crystallising phases in the MBS and UBS (apatite, quartz, alkali–feldspar); the higher proportion of dense minerals in the LS; the higher proportion of less dense minerals in the UBS – possibly

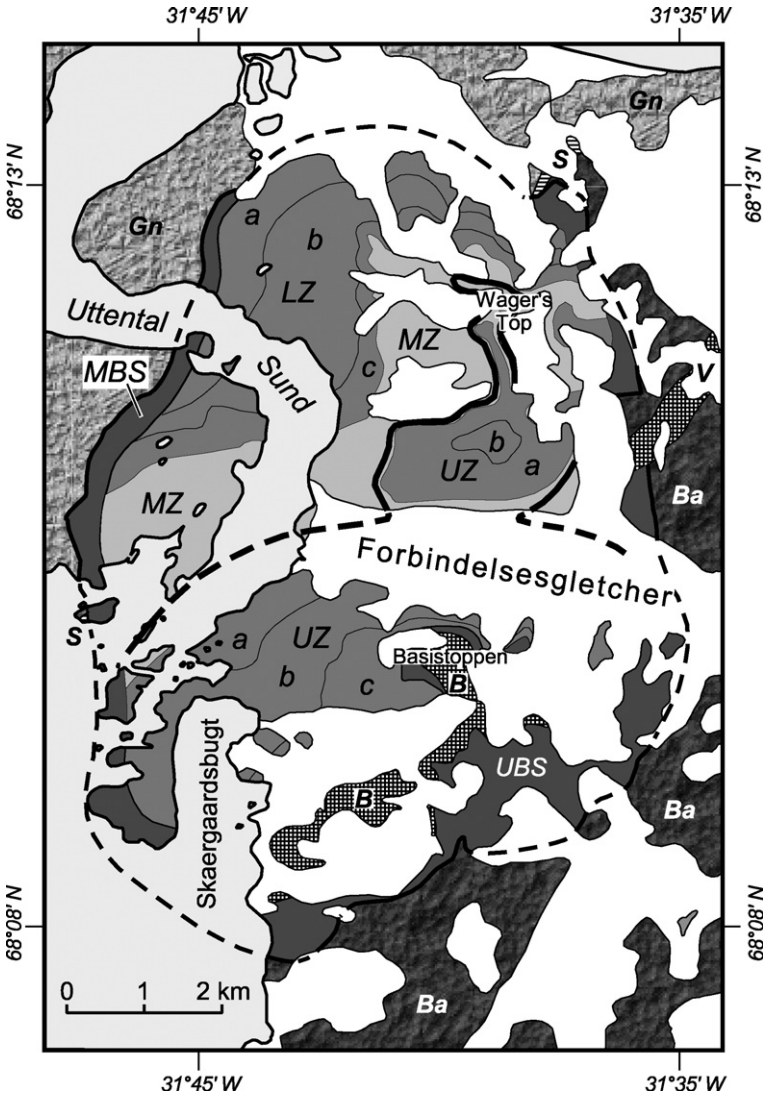

Fig. 1. Geological map of the Skaergaard Intrusion (after Wager and Brown, 1968; McBirney, 1989b). The gneissic basement (Gn), exposed to the North and West, is separated from the Palaeogene basalts (Ba), to the South and East, by a thin succession of Cretaceous sediments (S). The Southeastern parts of the Skaergaard Intrusion are crosscut by the Vandfaldsdalen Macrodike (V) and Basistoppen Sill (B). LZ(a,b,c), MZ, and UZ(a, b,c) refer to the Layered Series divisions; MBS and UBS to the Marginal and Upper Border Series respectively. The outcrop trace of the Platinova Reef is indicated by the solid line below the MZ–UZa boundary.

including units of anorthosite and granophyre (Irvine et al., 1998); and the slightly earlier appearance of cumulus mineral phases in the UBS than in the LS (cf., Naslund, 1984; Hoover, 1989b; Irvine et al., 1998; Nielsen, 2004). These differences concord with higher contents of interstitial liquid in the MBS and UBS and the differential settling of dense cumulus crystals to the LS.

2.1. Composition of the Skaergaard magma

A Skaergaard liquid line of descent was first determined by Wager and Deer (1939) and Wager (1960). They identified a preferred chilled margin composition (EG4507) to best represent the parental magma (Table 1). The magma evolution was calculated by the subtraction of relative volumes and compositions of cumulate units and yielded a trend of strong Fe-enrichment during crystallisation. This evolution trend, however, was challenged by Chayes (1970), who pointed out that mass balance on the cumulate units did not match the composition of the chilled margin. A gravity survey by Blank and Gettings (1973) showed that the Hidden Layered Series (also referred to as the Hidden Zone, HZ) was much smaller than calculated by

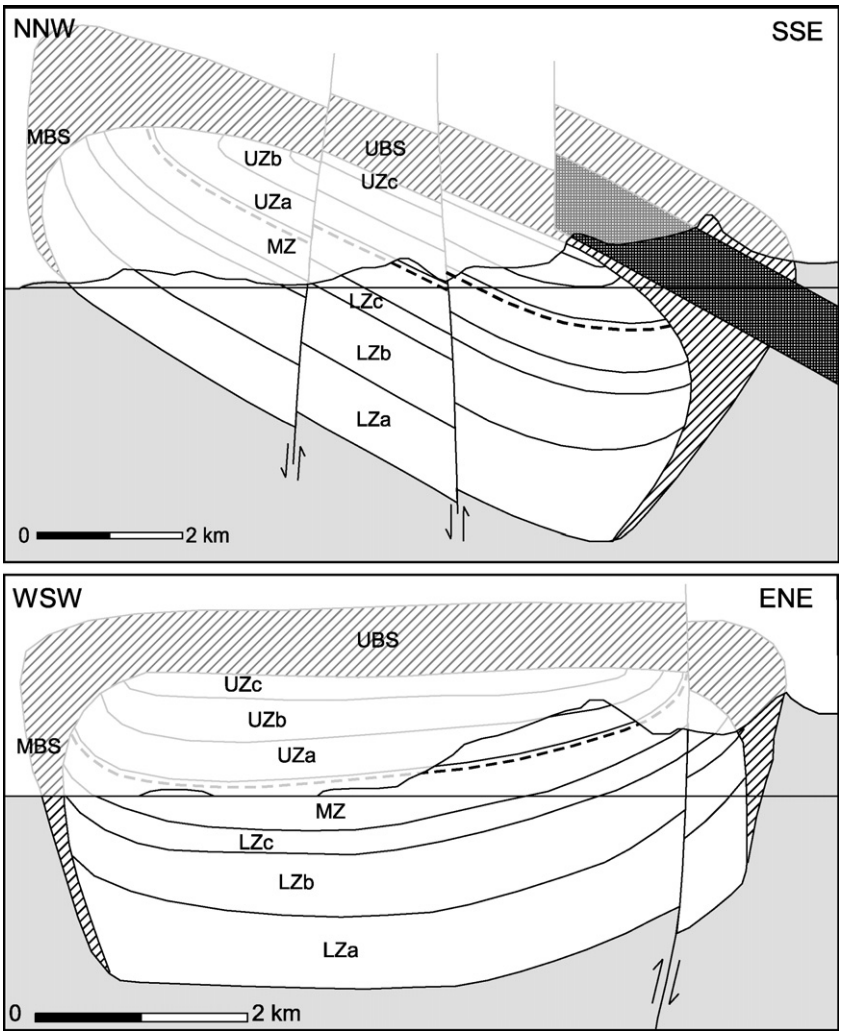

Fig. 2. Cross sections of the Skaergaard Intrusion showing the box-shaped, fault-bounded magma chamber (from Nielsen, 2004).

Wager (1960). This essentially removed the basis for the liquid line of descent determined by Wager (1960). Subsequently, alternative liquid lines of descent were proposed based on partial melting relations of cumulates by McBirney (1975); and by the association with a distinctive suite of "Skaergaard-like dykes" by Brooks and Nielsen (1978). Despite the apparent inconsistencies, all these evolution trends had been reasonably coherent. However, Hunter and Sparks (1987) challenged this by suggesting that the Skaergaard magma separated significant amounts of granophyric liquid during differentiation, and consequently that the alleged strong Fe-enrichment observed resulted from failure to incorporate this granophyre rather than being a true liquid line of descent.

The controversy about the Skaergaard liquid line of descent has largely grown out of the significant compositional variation of the chilled margin (Hoover, 1989a) and an incomplete knowledge of the relative volumes of the individual cumulate units. Liquid calculations have traditionally focused on the extent and composition of the HZ, although the extent and composition of the eroded parts are far more uncertain.

Recently, Nielsen (2004) provided a mass balance calculation of the intrusion based on a detailed study of the geometry and structural relations of the intrusion. His compilation was based on information gathered from outcrops and the Platinova drill cores; and an assumed polygonal, largely fault-controlled outline of the intrusion. His modeling yields a primary magma composition similar to high-Ti basalts exposed in the East Greenland flood basalt succession (Table 1). Although 5% granophyre has been added to the primary magma (assuming that some residual granophyre has

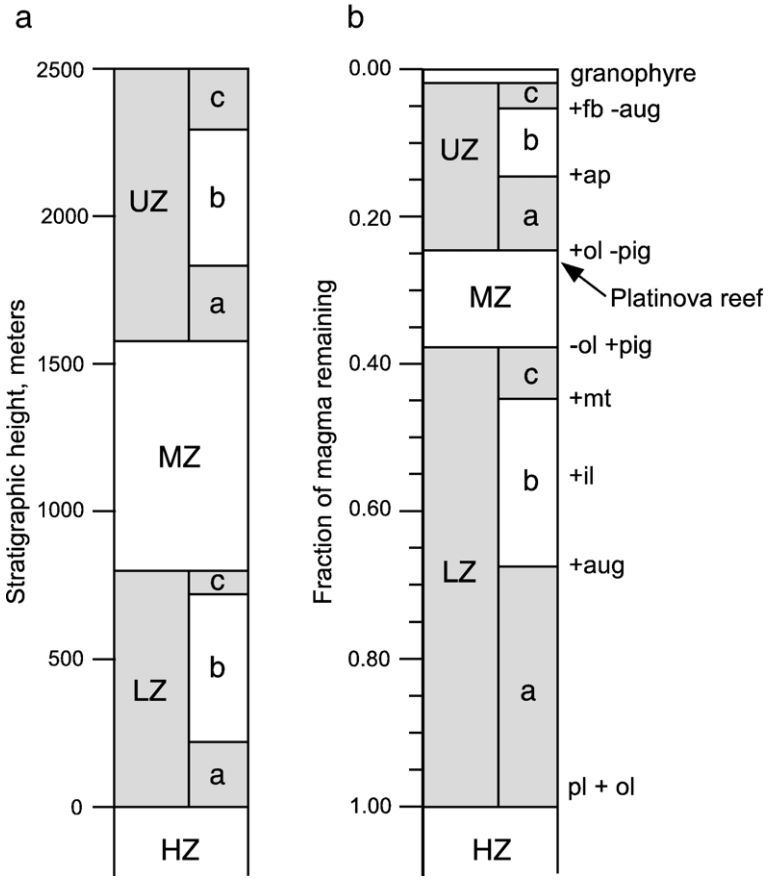

Fig. 3. Stratigraphy of the Skaergaard Layered Series: (a) lithologic column based on stratigraphic thicknesses from Wager and Brown (1968); (b) lithologic column based on relative volumes from Nielsen (2004). The fraction of magma remaining, *F*, is calculated by mass balance from the LZa parental magma. The appearance and disappearance of cumulus phases are indicated by + and − respectively. Mineral abbreviations as follows: pl=plagioclase, ol=olivine, aug=augite, il=ilmenite, mt=titanomagnetite, pig=pigeonite, ap=apatite, fb=ferrobustamite.

been lost), the magma is compositionally close to the KT-39 preferred chilled margin of Hoover (1989a). The main difference lies in the significantly higher FeO (total) content in the mass balance. However, although the FeO appears high, it is comparable to basalts in the East Greenland flood basalt province (Nielsen, 2004).

2.2. Sulphide minerals

Wager et al. (1957) identified that sulphide minerals in the Skaergaard Layered Series evolve from a Cu-rich assemblage dominated by bornite, blue chalcocite (or digenite), minor chalcopyrite and associated with non-titaniferous magnetite in MZ and the lower part of UZ, to a Fe-rich assemblage dominated by pyrrhotite (now extensively replaced by marcasite) with minor chalcopyrite in UZc. They reported the Cu-rich assemblage to nowhere exceed 0.05 modal % and the Fe-rich assemblage to average 2 modal %. Transgressive granophyres were reported to host pyrrhotite and pyrite. Wager et al. (1957, 1958) explained the Cu-rich, Ni-poor sulphide assemblage as a consequence of the late stage at which sulphide separation occurred (in contrast to the Ni-rich compositions of the Bushveld sulphides). Their analyses showed increased Cu and S concentrations at the level of the Triple Group, and they inferred that sulphur saturation had been reached certainly by the formation of UZa. This was confirmed by Turner (1986), who demonstrated distinct increases in the S content and the Cu/S around the base of the Triple Group (cf., Andersen et al., 1998).

The sulphide minerals in the Skaergaard Intrusion differ in both abundance and composition from sulphide minerals in intrusions hosting the classical PGE reefs (such as the Bushveld, Great Dyke, and Stillwater Complexes). Although they consequently may be considered unusual, similar mineral assemblages are found widespread in intrusions where sulphides are far less

Table 1
Suggested parental magmas to the Skaergaard Intrusion

	Wager and Brown (1968)	Hoover (1989a)	Nielsen (2004)	This study
	EG4507[a]	KT-39[a]	SK–TFDN	LZa–parent
SiO_2	48.08	49.69	47.91	47.51
TiO_2	1.17	2.66	3.09	2.98
Al_2O_3	17.22	13.21	13.80	13.35
FeO(total)	9.63	12.76	15.43	15.61
MnO	0.16	0.22	0.24	0.23
MgO	8.62	6.61	6.13	7.08
CaO	11.38	10.18	10.16	9.84
Na_2O	2.37	2.37	2.57	2.48
K_2O	0.25	0.56	0.40	0.39
P_2O_5	0.10	0.22	0.28	0.27
Total	98.98	98.48	100.01	99.73
Cu (ppm)	220[b]	n.d.	n.d.	250

n.d. = not determined.
[a] All Fe recalculated as FeO.
[b] Cu reported from Paster et al. (1974).

abundant (such as the Kap Edvard Holm Complex, East Greenland, Bird et al., 1995; intrusions in the Duluth Complex, Minnesota, Miller, 1999; Severson et al., 2002; and the Eastern Layered Series on the Isle of Rum, Hulbert et al., 1992; Butcher et al., 1999). As outlined by Miller and Andersen (2002), these differences are largely a result of the initial sulphur content of the parental magmas. Extensive crystallisation of olivine and magnetite has the effect of Ni-depletion prior to sulphur saturation, which coupled with incompatible behaviour of Cu in the magmas causes the sulphides in these intrusions to have less pentlandite and more chalcopyrite.

2.3. Noble metals

Noble metals in the Skaergaard were studied initially by Vincent and Smales (1956) and Vincent and Crocket (1960). Vincent and Smales (1956) reported 17 ppb Pd and 7 ppb Au in the Skaergaard chilled margin (EG4507). Vincent and Crocket (1960) investigated the fractionation of Au during the crystallisation of the LS. Their studies revealed minor enrichment of Pd and Au during the fractionation of the Skaergaard magma, although concentrations were generally low (2–9 ppb) and somewhat scattered. Although the data revealed no signs of mineralisation, scattered analyses of sulphide-bearing rocks showed elevated concentrations of 11–73 ppb. They concluded that the metals were excluded from the primary silicate and oxide minerals but showed a strong affinity to the Cu sulphides.

Andersen et al. (1998) published analyses of Pt, Pd, and Au through the LZ and MZ along with a compilation of Pd and Au analyses by Platinova A/S from the UZ. The analyses showed low concentrations of all elements throughout LZa and LZb (3–10 ppb Pt, 4–40 ppb Pd, and 2–12 ppb Au). The LZc and lower part of the MZ appear to be associated with increases in the abundances of Pt and Pd (5–25 ppb Pt, 27–153 ppb Pd), but not Au (which remains below 12 ppb). The upper part of the MZ hosts the Platinova Reef, and consequently has scattered concentrations up to (at least locally) 220 ppb Pt, 5.1 ppm Pd, and 9 ppm Au. Concentrations in the UZ rapidly decline to below the detection limit (1–2 ppb) for all elements, although scattered analyses of sulphide-bearing rocks still display up to 30 ppb Au.

2.4. The Platinova Reef

The Platinova Reef is a stratabound zone rich in Pd and Au that occurs in the uppermost 100 m of the MZ. The reef is associated with a succession of large-scale layers known as the Triple Group (Wager and Deer, 1939). The base of the reef, as described in publications by Bird et al. (1991), Andersen et al. (1998), and Nielsen (2001), appears to be perfectly concordant with the modal layering. The reef has a complex structure consisting of a succession of stratiform layers with elevated concentrations of Pd. The Pd concentrations become increasingly confined to the centre of the intrusion upward through the succession, and Au appears to occupy the fringes of these layers rather than forming a separate continuous reef. A fitting visual analogue to the geometry is a stack of Au-edged Pd-plates of decreasing size upwards. As a result, the dominant Pd and Au peaks show a systematic, although variable stratigraphic separation across the LS. The peaks nearly coincide at the margins but become increasingly detached inwards. At the centre of the intrusion, they show a maximum separation of some 60 m (Andersen et al., 1998).

Palladium and Au minerals occur mostly as alloys with Cu (skaergaardite and tetraauricuprite) that are closely associated with the Cu–Fe sulphides (Nielsen et al., 2003a,b,c,d,e; Rudashevsky et al., 2004). In most cases, the alloys are partially or completely enclosed by the sulphide minerals, suggesting that they are genetically related to the formation of the sulphides.

3. Constraints on sulphur, copper and noble metal solubilities

3.1. Sulphur solubility

The solubility of sulphur in mafic magmas strongly depends on the temperature, pressure, composition and

oxygen fugacity (Haughton et al., 1974; Poulson and Ohmoto, 1990; Mavrogenes and O'Neill, 1999). Parameters that are particularly important for the Skaergaard Intrusion are the iron-rich liquid line of descent (e.g., Wager, 1960; McBirney, 1975; Brooks et al., 1991; Toplis and Carroll, 1996; Tegner, 1997) and the inferred low oxygen fugacity (Morse et al., 1980; Sato and Valenza, 1980).

Sulphur is traditionally expected to enter silicate magmas in substitution for oxygen according to the relationship:

$$1/2S_2 + O^{2-} \leftrightarrow 1/2O_2 + S^{2-}. \quad (1)$$

For natural mafic magmas, in the absence of a gas phase, this is commonly interpreted to represent the reaction:

$$FeS_{sulphide} + O^{2-}_{silicate} \leftrightarrow FeO_{silicate} + S^{2-}_{silicate} \quad (2)$$

which yields a 1:1 atomic correlation between the sulphur solubility and FeO. This reaction was used by Haughton et al. (1974) to explain an observed positive correlation between the FeO and S concentrations of sulphur saturated basalts, and it was recently applied to the Bushveld Complex, South Africa, by Li et al. (2001).

Poulson and Ohmoto (1990) observed a distinct difference between iron-poor and iron-rich magmas which they related to a change in the sulphur speciation of the magmas at around 10 wt.% FeO. Where iron-poor magmas were found to be in agreement with the 1:1 S to FeO relationship expected from Eq. (2) (although very strongly influenced by temperature), iron-rich magmas showed a strong positive FeS to FeO correlation (yielding a 1:2 slope in a plot of $\log X^{FeO}$ and $\log X^{S}$). They suggested this to reflect the following reaction:

$$FeS + 2FeO \leftrightarrow Fe_3SO_2. \quad (3)$$

During the closed system Skaergaard fractionation, the formation of sulphide liquid reflects a balance between the sulphur concentration and the evolution in sulphur saturation (thus the FeO concentration) during magmatic differentiation. Thus, an iron-enrichment trend during fractionation (Fenner-type differentiation) would generally be expected to delay sulphur saturation in comparison with magmas undergoing silica-enrichment (Bowen-type differentiation). Furthermore, a low oxygen fugacity (f_{O_2}) (as expected during closed system fractional crystallisation; Osborn, 1959) is expected to increase the solubility of sulphur according to the following reaction (cf., Poulson and Ohmoto, 1990):

$$S^{2-} + 3FeO_{silicate} \leftrightarrow Fe_3SO_{2silicate} + O^{2-}. \quad (4)$$

A low oxygen fugacity will drive this reaction to the right to reduce the amount of free sulphur and liberate oxygen in the magma. The iron-enrichment trend and the low f_{O_2} give strong reasons for substantial fractionation of the Skaergaard magma before sulphur saturation was reached. This is significant because it allows for substantial enrichment of incompatible noble metals (PGE, Au) during magmatic differentiation before their collection by immiscible sulphide liquid droplets (as also observed for Pd in the East Greenland flood basalts by Momme et al., 2002).

The effects of pressure and temperature on the sulphur solubility was explored by Mavrogenes and O'Neill (1999). They found the following relationship for the pressure and temperature dependence of the sulphur solubility of mafic magmas:

$$\ln C^S = \frac{A}{T} + B\frac{CP}{T} + \ln a^{sulphide}_{FeS} \quad (5)$$

where C^S is the sulphur concentration at saturation in ppm, A, B, and C are constants, T is the temperature in K, and P the pressure in bar. The activity coefficient, $a^{sulphide}_{FeS}$, was considered to be approximately 1 (Mavrogenes and O'Neill, 1999). Using their constants for synthetic basalt (their Table 3): $A=-6684$, $B=11.52$, $C=-0.047$, the overall effect of temperature between 1373 and 1473 K can be approximated by 3 ppm/K, the overall effect of pressure amounts to −33 ppm/kbar. For this restricted temperature range, Eq. (5) can thus be simplified by the linear approximation:

$$C^S(P,T)\ [\text{ppm}] = C^S(1473\ \text{K},1\ \text{bar}) - 3(1473 - T) - 0.0033P. \quad (6)$$

3.2. Cu and noble metal solubilities

Bird et al. (1991) suggested that the Au in the Platinova Reef formed from an immiscible liquid metal that became trapped in interstitial silicates. They considered this liquid metal to be separate from the sulphide-rich liquid. Because of this and the unusual Cu-rich composition of the Skaergaard sulphides, a brief discussion of Cu and noble metal solubilities is appropriate.

The effect of Cu and the noble metals on the sulphur solubility and composition of immiscible sulphide liquids is unfortunately only poorly known. Experiments by Holzheid and Lodders (2001) and Ripley et al. (2002) indicate that Cu solubilities are strongly influenced by the sulphur fugacities of magmas.

Holzheid and Lodders (2001) reported solubilities of 440 to 3378 ppm in basalts in equilibrium with both sulphide and metal. For sulphur-poor basaltic systems without the presence of metal, Ripley et al. (2002) reported solubilities from 594 to 1550 ppm. Additionally, they showed that magmas extremely rich in Cu (aluminous olivine basalts doped with 2 and 10 wt.% Cu) may yield sulphide liquids compositionally between chalcopyrite and bornite. Both papers, unfortunately, only deal with basalts of very restricted compositional variation, none of them reaching the Fe-rich compositions similar to the evolved Skaergaard magma at the MZ–UZ boundary. It is therefore difficult to assess any consequences for sulphur saturation or the composition of the Skaergaard sulphide liquids.

The solubilities of PGE and Au in basaltic magmas were investigated by Borisov and Palme (1996, 1997, 2000). Borisov and Palme (2000) reported solubilities at 0.4 ppm Au and 3 ppm Pd at 1473 K (1200 °C). These values were unfortunately measured in a FeO-free experimental system. Bearing in mind the strong geochemical affinity of the PGE to Fe, solubilities are likely to be higher in natural magmas, and most likely of little consequence to the sulphur saturation.

4. Modeling parameters

4.1. Skaergaard magma evolution

Although this paper does not attempt to resolve the controversy on the Skaergaard liquid line of descent, a coherent model is required for the magma evolution. For each element, the concentration in the parental magma can be calculated by mass balance according to the following equation:

$$C_L = \sum_{i=1}^{n} w_i \cdot C_i \quad (7)$$

Collected relative mass proportions (Nielsen, 2004) and average compositions (McBirney, 1989a) of lithological units (zones) have been added up to yield a parental magma for LZa (Table 2). As recommended by Nielsen (2004), 5 wt.% melanogranophyre was added to the bulk composition of the cumulates. The composition obtained at this level has been assumed to represent the parental magma for the later cumulate units. Note that the parental magma used here does not include the HZ or the 3 wt.% olivine cumulates estimated by Nielsen (2004) to have fractionated prior to the base of LZa (part of his SK–TFDN parental liquid composition, Table 1). As such, it is not a parental magma for the intrusion and is independent of the extent and composition of the HZ.

Table 2
Lithological compositions (from McBirney, 1989a) and calculated parental magma used for the numerical modeling

	LZa equivalents			LZb equivalents			LZc equivalents			MZ equivalents			UZa equivalents			UZb equivalents			UZc equivalents		Melanogranophyre	LZa parental magma
	LZa	MBS LZa	UBSα1	LZb	MBS LZb	UBSα	LZc	MBS LZc	UBSα2	MZ	MBS MZ	UBSβ	UZa	MBS UZa	UBSγ1	UZb	MBS UZb	UBSγ2	UZc	UBS γ3		
Mass proportion[a]	23.97	5.84	4.65	16.65	3.90	3.16	5.44	1.27	0.97	9.79	2.31	1.85	7.24	1.72	1.31	5.94	1.27	1.07	1.38	0.28	5.26	105.26
Mass percentage	22.83	5.56	4.43	15.86	3.71	3.01	5.18	1.21	0.92	9.32	2.20	1.76	6.89	1.64	1.25	5.66	1.21	1.02	1.31	0.27	5.00	100.00
SiO_2	48.12	49.43	49.47	48.84	50.30	49.58	41.10	44.86	49.68	42.79	43.46	46.99	43.07	44.33	51.96	41.78	47.99	53.86	46.00	51.55	62.18	47.51
TiO_2	1.35	1.00	2.33	1.44	1.08	2.41	6.92	4.91	2.48	6.79	5.44	4.47	5.67	6.24	2.51	4.06	3.49	1.98	2.63	1.50	1.07	2.98
Al_2O_3	16.81	13.71	16.81	12.55	14.13	16.20	11.02	11.35	15.69	11.53	12.48	12.98	11.17	10.05	13.12	9.51	8.28	11.96	7.86	8.92	12.41	13.35
FeO(total)	11.13	11.87	10.76	12.84	11.83	11.11	21.10	19.02	11.45	20.00	20.51	15.62	22.52	21.47	14.90	26.64	26.11	16.49	28.67	23.00	12.37	15.61
MnO	0.16	0.19	0.17	0.21	0.18	0.17	0.26	0.26	0.17	0.26	0.23	0.20	0.31	0.29	0.21	0.41	0.40	0.23	0.65	0.29	0.20	0.23
MgO	9.42	10.77	4.58	10.13	9.42	4.68	7.61	6.60	4.78	6.24	5.64	4.89	5.62	5.57	1.87	3.41	2.11	0.95	0.38	0.14	0.10[b]	7.08
CaO	10.11	10.76	10.49	11.57	10.89	10.36	9.77	10.59	10.23	9.87	9.54	9.48	8.62	9.39	7.94	9.36	6.77	6.58	10.14	8.51	4.65	9.84
Na_2O	2.52	1.93	3.00	2.13	1.88	3.00	1.97	2.03	3.00	2.23	2.24	2.69	2.55	2.08	3.54	2.59	2.11	3.85	2.42	2.87	4.19	2.48
K_2O	0.27	0.25	0.41	0.20	0.22	0.40	0.20	0.26	0.38	0.21	0.35	0.57	0.26	0.34	0.98	0.36	1.12	1.30	0.41	0.82	1.99	0.39
P_2O_5	0.11	0.08	0.18	0.09	0.07	0.21	0.05	0.13	0.23	0.08	0.12	0.21	0.22	0.24	0.84	1.88	1.62	0.69	0.84	0.29	0.31	0.27
Total	100.00	99.99	98.20	100.00	100.00	98.12	100.00	100.01	98.09	100.00	100.01	98.10	100.01	100.00	97.87	100.00	100.00	97.89	100.00	97.89	99.47	99.73
Cu (ppm)	118	116	207	105	91	207	101	143	205	122[c]	126	292	1005	370	477	794	921	383	450	116	131	250

Mass proportions and notations from Nielsen (2004). The mass percentages used in the mass balance modeling are calculated to incorporate 5% melanogranophyre.

[a] From Nielsen (2004).

[b] The best available melanogranophyre has 0.63 wt.% MgO, which is less evolved than the UZc and SH. The value has for the purposes of the modeling been reduced to 0.10 wt.%.

[c] Average calculated from data by McBirney (1998).

Progressive Skaergaard liquid compositions were calculated by the stepwise subtraction of equivalent LS, MBS, and UBS lithologies from the initial magma composition. Values of F (the fraction of liquid remaining) are determined by the successive subtraction of lithological zone mass proportions (in fractions rather than percents) with $F=1$ at the base of LZa. To obtain more data points, the subtraction has been carried out in increments at the base and middle of each lithological zone (this assumes that the compositional evolution within each individual zone is small). Unfortunately the average copper concentration from the MZ reported by McBirney (1989a) appears to include some sulphur saturated rocks, and consequently an average has been used of concentrations below 300 ppm (yielding 122 ppm) from McBirney (1998). This estimate is more in line with the concentrations in LZ.

For the calculations below, the magma has been assumed to be homogeneous throughout the crystallisation. This is justified by the broad compositional similarities between the LS and UBS (cf., Irvine et al., 1998). The fact that Pd and Au appears to have been almost completely scavenged from the entire magma body to form the Platinova Reef (Andersen et al., 1998) justifies the assumption that sulphur saturation occurred throughout the magma body at the same time. Melanogranophyre was subtracted throughout UZ, with 1 wt.% in each of the three subzones, and 2 wt.% residual after fractionation of the Sandwich Horizon.

Crystallisation of the cumulus minerals is likely to have occurred between 1.5 kbar at the base of the Skaergaard Intrusion and around 0.5 kbar at the SH with intercumulus crystallisation continuing under increasing pressure to 2.5 kbar at the SH (cf., Lindsley et al., 1969; Larsen and Tegner, 2006). For the present calculations, a constant pressure of 1 kbar has been used. The liquidus temperatures of dry successive magmas were calculated with the MELTS program (Ghiorso and Sack, 1995) using a Fe_2O_3/FeO mass ratio of 0.15.

The effect of contamination was modeled on the LZa initial magma by assuming a contaminant partial melt from the basement equivalent to the composition of the felsic component of the Tinden Sill granophyre (sample EG3058 of Wager and Deer, 1939). As sulphur could have been mobilised, the modeling is carried out for concentrations within the range 0–1000 ppm.

4.2. Fractionation of Cu and S

Below the level of sulphur saturation, Cu and S can be expected to be incompatible during crystallisation of the cumulus minerals following the relationships for Rayleigh fractionation:

$$C_L = C_0 F^{(D-1)} \tag{8}$$

$$C_S = DC_L \tag{9}$$

This formula is independent of the starting point for fractionation, as long as the values of F and C_0 are coordinated. For cumulate rocks, the bulk partition coefficient (D) of incompatible elements will greatly reflect the amount of trapped liquid (W_{TL}) and is calculated by the following equation:

$$D = D_{\text{cumulus}} \cdot (1 - W_{TL}) + W_{TL} \tag{10}$$

Consequently, to allow for variable partition coefficients, the calculations are based on a step-wise fractionation model using the determined concentrations of the latest magma as parental magma for the subsequent fractionation increment. From step 1 to step 2, Eq. (8) thus is modified to:

$$C_{L,2} = C_{L,1} \cdot \left(\frac{F_2}{F_1}\right)^{(D_1-1)} \tag{11}$$

Unfortunately partition coefficients for Cu and S are poorly explored, but their geochemical behaviour can, to some extent, be estimated from their ionic radii and charges. Differences in the ionic radii will largely prevent S^{2-} from substituting for O^{2-} in silicate and oxide minerals, and S^{2-} is consequently expected only to be accommodated by accidental inclusion yielding a $D^S_{\text{cumulus}} \approx 0$. As such, following Eq. (10), the S concentrations in the cumulates are expected to largely reflect the amount of trapped liquid. In contrast, Cu^{2+} would be expected more readily to substitute for Mg^{2+} and Fe^{2+} and thus be expected to enter ferromagnesian minerals to some extent. The partition coefficient for Cu in olivine was determined between 0.075 and 0.19 for komatiitic magmas by Gaetani and Grove (1997). Onuma diagrams suggest higher partition coefficients for augite (cf., Henderson, 1982). In the modeling below, the Cu concentration is constrained by mass balance evolution and a bulk cumulus partition coefficient inferred by fitting the mass balance evolution to a Rayleigh fractionation curve. Consequently for Cu, C_0 and D have been modeled to match the magma evolution as determined by mass balance; for S, C_0 has been adjusted to match sulphur saturation in the upper part of MZ using a bulk partition coefficient, $D=W_{TL}$. The amount of trapped liquid has been estimated from

Table 3
Magma compositions calculated by successive removal of bulk cumulates

	LZa-base	LZa-mid	LZa-LZb	LZb-mid	LZb-LZc	LZc-mid	LZc-MZ	MZ-mid	MZ-UZa	UZa-mid	UZa-UZb	UZb-mid	UZb-UZc	UZc-mid	SH
F	1.0000	0.8363	0.6727	0.5600	0.4474	0.4109	0.3745	0.3082	0.2419	0.1907	0.1394	0.0976	0.0557	0.0454	0.0200
Height	0	110	220	475	730	765	800	1190	1580	1710	1840	2060	2280	2390	2500
SiO_2	47.51	47.31	47.01	46.58	45.92	46.20	46.53	47.19	48.21	49.00	50.36	52.51	57.87	59.53	62.18
TiO_2	2.98	3.29	3.74	4.19	4.86	4.76	4.64	4.29	3.75	3.37	2.71	2.35	1.46	1.31	1.07
Al_2O_3	13.35	12.78	11.92	11.65	11.23	11.19	11.15	10.99	10.75	10.60	10.35	10.59	11.17	11.65	12.41
FeO (total)	15.61	16.47	17.75	18.82	20.42	20.50	20.59	20.82	21.19	21.25	21.37	20.04	16.71	15.04	12.37
MnO	0.23	0.24	0.26	0.27	0.29	0.29	0.30	0.31	0.32	0.33	0.35	0.34	0.31	0.27	0.2
MgO	7.08	6.71	6.15	5.52	4.57	4.35	4.08	3.68	3.05	2.56	1.70	1.26	0.17	0.14	0.1
CaO	9.84	9.75	9.63	9.29	8.78	8.68	8.55	8.30	7.89	7.74	7.47	7.09	6.13	5.56	4.65
Na_2O	2.48	2.48	2.48	2.53	2.62	2.66	2.72	2.81	2.95	3.02	3.15	3.31	3.71	3.90	4.19
K_2O	0.39	0.41	0.44	0.48	0.55	0.57	0.61	0.68	0.78	0.88	1.03	1.18	1.56	1.73	1.99
P_2O_5	0.27	0.30	0.35	0.39	0.47	0.50	0.54	0.64	0.78	0.91	1.14	0.94	0.43	0.39	0.31
Total	99.73	99.73	99.72	99.72	99.71	99.70	99.70	99.69	99.67	99.66	99.63	99.60	99.52	99.50	99.47
Cu (ppm)	250	274	309	348	406	431	462	530	635	593	521	430	205	169	131
T_L (K)	1449.62	1437.96	1427.51	1421.75	1412.47	1410.22	1407.58	1401.43	1391.76	1384.44	1372.76	1368.95	1367.49	1368.17	1370.42
W_{TL} (wt.%)	47.70	40.36	33.03	27.98	22.93	21.29	19.66	16.69	13.72	11.42	9.12	7.24	5.37	4.90	3.77

Stratigraphic height in m (after Wager and Brown, 1968), concentrations in wt.%. *F* represents the fraction of magma remaining, as calculated from the mass balance. T_L represent liquidus temperatures calculated by the Melts program (Ghiorso and Sack, 1995), and W_{TL} the estimated trapped liquid in wt.%.

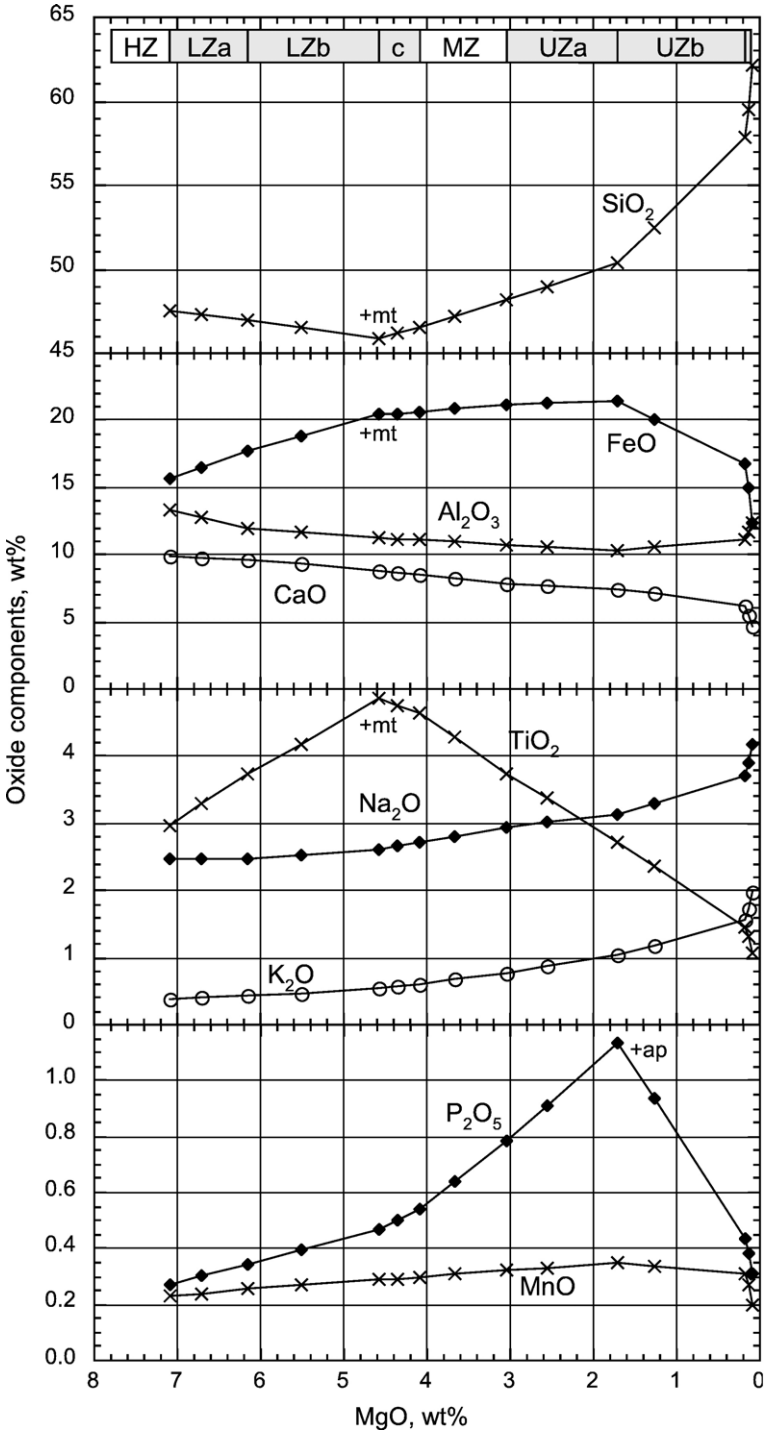

Fig. 4. Variation diagrams of the modeled Skaergaard magma evolution. All Fe is included as FeO. Notable changes in the trends relate to the crystallisation of titanomagnetite (+mt) and apatite (+ap). Data are presented in Table 3.

the concentrations of P_2O_5, which can be assumed to be perfectly incompatible in the cumulus minerals until apatite reaches its liquidus in UZb.

When sulphur saturation is reached, the further Cu evolution is determined by mass balance and the S concentration is constrained by the evolution in the

sulphur saturation level. Following Bowen's original principles for the saturation of coexisting liquids in equilibrium (Bowen, 1928), it is assumed that the magma remains at the point of sulphur saturation throughout the remaining differentiation, and that the excess sulphur forms an immiscible sulphide liquid. Although neither silicate nor sulphide liquids are stoichiometric compounds; Cu, Fe, and S are major elements (exceeding the upper limit for Henry's Law behaviour) in the sulphide liquids and subject to the effects of closure (Chayes, 1971), consequently their concentrations are expected to be strongly interdependent. Sulphide–silicate partition coefficients for these elements must consequently be taken only as rough indicators of their geochemical behaviour.

4.3. Sulphur saturation

Sulphur saturation has been calculated using the relationship with FeO in iron-rich magmas (more than around 10 wt.% FeO) given by Poulson and Ohmoto (1990). They suggested the following correlation between the molar fractions of sulphur (X^{S}) and FeO (X^{FeO}) at the saturation level:

$$\log X^{S} = -0.8 + 2.0 \log X^{FeO} \quad \text{(at 1473 K,1 bar)} \tag{12}$$

The saturation concentration has been adjusted for temperature and pressure effects using Eq. (6). An excess of sulphur in the magma above this level is expected to produce an immiscible sulphide liquid.

4.4. Sulphide liquid composition

The sulphide liquid composition has been assumed to be compositionally similar to a mixture of chalcopyrite ($CuFeS_2$) and pyrrhotite ($Fe_{0.95}S$) in accordance with the Cu-rich, Ni-poor composition of the Skaergaard magma at the MZ–UZ boundary. This is based on the assumption that Fe is the major cation in the sulphide liquid apart from Cu. Assuming fixed (Cu+Fe)/S of the chalcopyrite and pyrrhotite, with known Cu and S concentrations, the remaining Fe can be calculated by difference.

The amount of Cu and S in the cumulate have been estimated by matching the rate of change in the concentrations of the elements in the magma (for Cu from the mass balance curve, for S from the incompatible fractionation and sulphur saturation curves) to bulk cumulate–magma partition coefficients. The concentrations can be matched to the ideal mineral compositions of chalcopyrite and pyrrhotite to calculate the expected sulphide mineral abundances and assemblages. The S/Cu ratio of the magma before sulphide saturation is allowed to evolve according to the differences in bulk partition coefficients between the elements. After sulphur saturation, it is assumed that the S/Cu ratio is controlled by the composition of the sulphide melt.

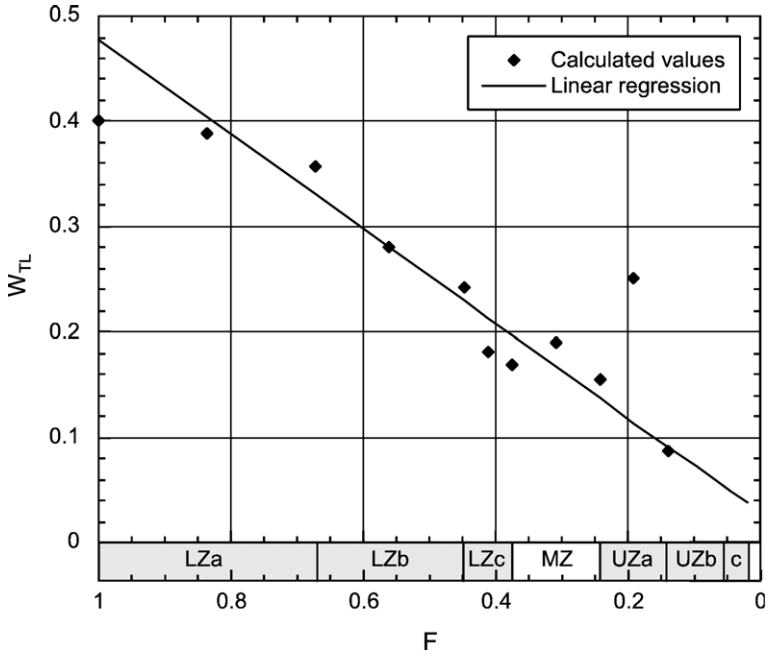

Fig. 5. The amount of trapped liquid calculated from the P_2O_5 concentrations for successive lithological units in the LS. The evolution has been approximated by linear regression to *F*.

5. Results

5.1. Evolution of the Skaergaard magma

In the mass balance modeling presented here, the Skaergaard magma evolves from an evolved iron-rich tholeiitic basalt, through a ferrodiorite, to a granophyre during the course of crystallisation (Table 3 and Fig. 4). Liquidus temperatures for the dry magmas decrease from 1450 K at the base of LZa to around 1368 K in UZc (Table 3). The evolution trend through LZa and LZb displays strong Fe-enrichment and mild Si-depletion during fractionation. The onset of titanomagnetite crystallisation decreases the rate of Fe-enrichment, although FeO continues to increase through MZ and UZa. A pronounced Si-enrichment is initiated at the base of LZc – a trend that continues throughout the remaining course of crystallisation. The mass balance yields 1.14 wt.% P_2O_5 at the level of apatite saturation, which is consistent with the 1.0 to 1.6 wt.% estimated for the Bushveld Upper Zone by Cawthorn and Walsh (1988).

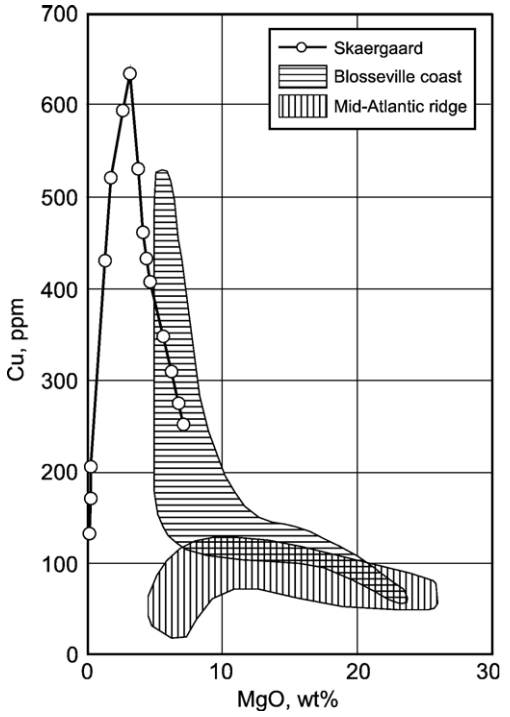

Fig. 6. Cu-fractionation of the Skaergaard magma, as calculated by mass balance, in relation to uncontaminated flood basalts from the East Greenland coast (data from Larsen et al., 1989 and Momme et al., 2002; as synthesised by Andersen et al., 2002). The fractionation trend of North Atlantic N-MORB (based on data from the Deep Sea Drilling Project leg 37) is included for comparison. Data are presented in Table 3.

Table 4
Input parameters and results of sulphide saturation calculations

	LZa-base	LZa-mid	LZa-LZb	LZb-mid	LZb-LZc	LZc-mid	LZc-MZ	MZ-mid	MZ-UZa	UZa-mid	UZa-UZb	UZb-mid	UZb-UZc	UZc-mid	SH
F	1.0000	0.8363	0.6727	0.5600	0.4474	0.4109	0.3745	0.3082	0.2419	0.1907	0.1394	0.0976	0.0557	0.0454	0.0200
FeO (wt.%)	15.61	16.47	17.75	18.82	20.42	20.50	20.59	20.82	21.19	21.25	21.37	20.04	16.71	15.04	12.37
W_{TL} (wt.%)	47.70	40.36	33.03	27.98	22.93	21.29	19.66	16.69	13.72	11.42	9.12	7.24	5.37	4.90	3.77
T_L [K]	1449.62	1437.96	1427.51	1421.75	1412.47	1410.22	1407.58	1401.43	1391.76	1384.44	1372.76	1368.95	1367.49	1368.17	1370.42
S ($D=W_{TL}$) (ppm)	894	995	1151	1313	1561	1669	1799	2116	2607	3219	4280	5958	10120	12311	27074
$\log\gamma^{FeO}$	−0.8608	−0.8366	−0.8027	−0.7747	−0.7353	−0.7330	−0.7304	−0.7245	−0.7156	−0.7131	−0.7088	−0.7367	−0.8155	−0.8614	−0.9462
$\log\gamma^{S}$	−2.7523	−2.7051	−2.6403	−2.5804	−2.5014	−2.4717	−2.4386	−2.3672	−2.2751	−2.1823	−2.0568	−1.9130	−1.6829	−1.5978	−1.2556
$\log K^{S}$ (saturation)	−2.5523	−2.5101	−2.4443	−2.3874	−2.3072	−2.3036	−2.2992	−2.2897	−2.2751	−2.2733	−2.2696	−2.3353	−2.5244	−2.6406	−2.8760
S-saturation (ppm)	1417	1558	1807	2048	2441	2459	2480	2529	2607	2611	2621	2253	1457	1115	649

The amount of trapped liquid has been estimated from the P_2O_5 evolution of the magma. This has been done by matching increments in the P_2O_5 evolution of the magma (determined from the mass balance, Table 3) to a Rayleigh fractionation curve (by using Eq. (11)). When assuming a $D_{cumulus} \approx 0$ for P_2O_5, the successive bulk partition coefficients derived (following Eq. (10)) will be equal to the successive fractions of trapped liquid. From this, a systematic decrease in the amount of trapped liquid is observed during crystallisation (Fig. 5). This evolution can be approximated by linear regression to a straight line following the equation:

$$W_{TL} = 0.028707 + 0.44832F \quad (R^2 = 0.943) \qquad (13)$$

The result shows a systematic decrease from around 48 wt.% trapped liquid at the base of LZa through 14 wt.% at the MZ–UZ boundary to around 7.5 wt.% in UZc. These estimates are comparable to values calculated by Paster et al. (1974).

The mass balance outlined above yields an initial Cu concentration (C_0^{Cu}) of 250 ppm increasing to a maximum of 635 ppm at the MZ–UZa boundary before dropping off to 131 ppm at the SH (Table 3). The fractionation trend is comparable to that of evolved East Greenland plateau basalts (Andersen et al., 2002; Momme et al., 2002), except that the Skaergaard magma evolves to higher concentrations (Fig. 6).

5.2. Sulphur saturation induced by magmatic fractionation

The level of sulphur saturation in the intrusion was calculated by first converting the mass proportions of the successive magmas to molar proportions. From this, the molar proportion of FeO (X^{FeO}) was extracted for calculation of the compositionally dependent sulphur solubility using Eq. (12). The resulting molar fractions of sulphur at saturation (X^S) were converted to weight proportions (in ppm) and modified for temperature and pressure effects following Eq. (6) to yield the evolution in sulphur solubility presented in Table 4 and Fig. 7. Corresponding concentrations of S and Cu in progressive Skaergaard magmas and cumulates are presented in Table 5.

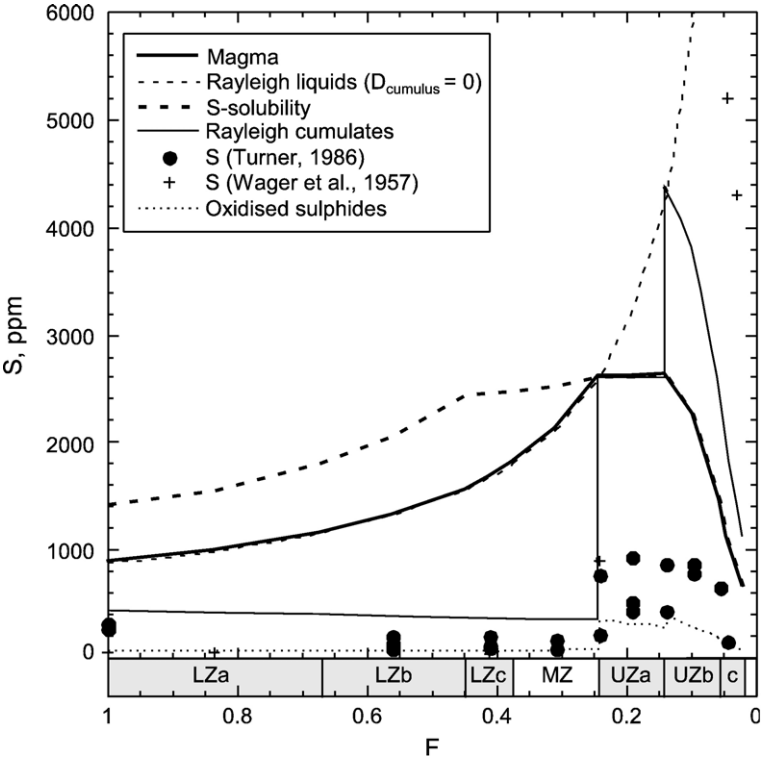

Fig. 7. Variations in the S-concentration as a function of *F*. The evolution prior to sulphur saturation is modeled along the curve of incompatible fractionation using a $D^S = W_{TL}$. The fractionation after sulphur-saturation follows the sulphur solubility curve. Expected concentrations in the cumulates prior to sulphur saturation are calculated with similar parameters, concentrations after saturation by fitting the magma evolution to the slope of the saturation curve yielding a $D^S_{cumulus} = 0.99$ through UZa and $D^S_{cumulus} = 1.74$ through UZb and UZc. Data are presented in Tables 4 and 5.

Table 5
Calculated Cu and S concentrations in magma and cumulate during fractionation in the Skaergaard Intrusion

Before S-saturation	LZa-base	LZa-mid	LZa-LZb	LZb-mid	LZb-LZc	LZc-mid	LZc-MZ	MZ-mid	MZ-top
F	1.0000	0.8363	0.6727	0.5600	0.4474	0.4109	0.3745	0.3082	0.2419
Cu (magma, mass balance)	250	274	309	348	406	431	462	530	635
Cu (magma, $D_{cumulus}$=0.13)	250	275	312	350	407	431	460	530	635
Cu (cumulate)	151	150	153	158	168	173	179	194	219
S (magma, $D=W_{TL}$)	894	995	1151	1313	1561	1669	1799	2116	2607
S (cumulate)	427	402	380	367	358	355	354	353	358
S (oxidised cumulate)	61	60	61	63	67	69	72	78	88
S/Cu (magma)	3.57	3.62	3.69	3.75	3.84	3.87	3.91	3.99	4.10
S/Cu (cumulate)	2.83	2.67	2.48	2.32	2.13	2.05	1.97	1.82	1.64

After S-saturation	UZa-base	UZa-mid	UZa-top	UZb-base	UZb-mid	UZb-UZc	UZc-mid	SH
F	0.2419	0.1907	0.1394	0.1394	0.0976	0.0557	0.0454	0.0200
Cu (magma, mass balance)	635	593	521	521	430	205	169	131
Cu (magma, $D_{cumulus}$=0.13)	635	763	978	978	1304	2067	2452	4866
Cu (cumulate)	854	791	710	947	710	445	374	185
S (magma, saturation)	2607	2611	2621	2621	2253	1457	1115	649
S (cumulate)	2584	2588	2598	4384	3800	2478	1900	1111
S (oxidised cumulate)	345	319	287	382	286	179	151	75
S/Cu (magma)	4.10	4.40	5.04	5.04	5.23	7.10	6.58	4.95
S/Cu (cumulate)	3.02	3.27	3.66	4.63	5.35	5.57	5.09	6.01

Concentrations in ppm.

An initial sulphur concentration (C_0^S) of 894 ppm is required for the Skaergaard magma to reach sulphur saturation in the upper part of MZ (Tables 4–6; Fig. 7). At the level of saturation, the magma is modeled to contain 635 ppm Cu and 2607 ppm S. This is equivalent to the formation of around 0.71 wt.% (0.53 modal %) sulphide on average throughout UZ. During sulphur unsaturated fractionation, the Cu evolution matches closely a Rayleigh fractionation model provided a small amount of Cu is incorporated into the cumulus minerals (corresponding to a $D_{cumulus}^{Cu}$ of 0.13) (Table 5 and Fig. 8). Because of this higher bulk partition coefficient of Cu than S, the modeling yields an increasing S/Cu ratio. Assuming the Cu to be incorporated into

Table 6
The primary sulphide paragenesis assuming a chalcopyrite–pyrrhotite assemblage

	Sulphide abundance (wt.%)	Sulphide abundance (modal %)	S/Cu (sulphide)	Sulphide composition		Percent of S in chalcopyrite
				Chalcopyrite	Pyrrhotite	
LZa-base	0.116	0.079	3.57	29.8	70.2	28.3
LZa-mid	0.109	0.075	3.62	29.4	70.6	27.9
LZa-LZb	0.103	0.073	3.69	28.9	71.1	27.3
LZb-mid	0.100	0.070	3.75	28.4	71.6	26.9
LZb-LZc	0.097	0.073	3.84	27.8	72.2	26.3
LZc-mid	0.096	0.072	3.87	27.5	72.5	26.1
LZc-MZ	0.096	0.071	3.91	27.3	72.7	25.8
MZ-mid	0.096	0.070	3.99	26.7	73.3	25.3
MZ-top	0.097	0.071	4.10	26.0	74.0	24.6
UZa-base	0.704	0.526	3.02	35.1	64.9	33.4
UZa-mid	0.703	0.524	3.27	32.5	67.5	30.8
UZa-top	0.704	0.523	3.66	29.1	70.9	27.6
UZb-base	1.184	0.887	4.63	23.1	76.9	21.8
UZb-mid	1.024	0.765	5.35	20.0	80.0	18.8
UZb-UZc	0.667	0.500	5.57	19.2	80.8	18.1
UZc-mid	0.512	0.384	5.09	21.1	78.9	19.8
SH	0.299	0.191	6.01	17.9	82.1	16.8

Note the changes related to the sulphur saturation at the base of UZa.
Where not otherwise noted, concentrations are in weight percent, the S/Cu is the mass ratio in the magma.

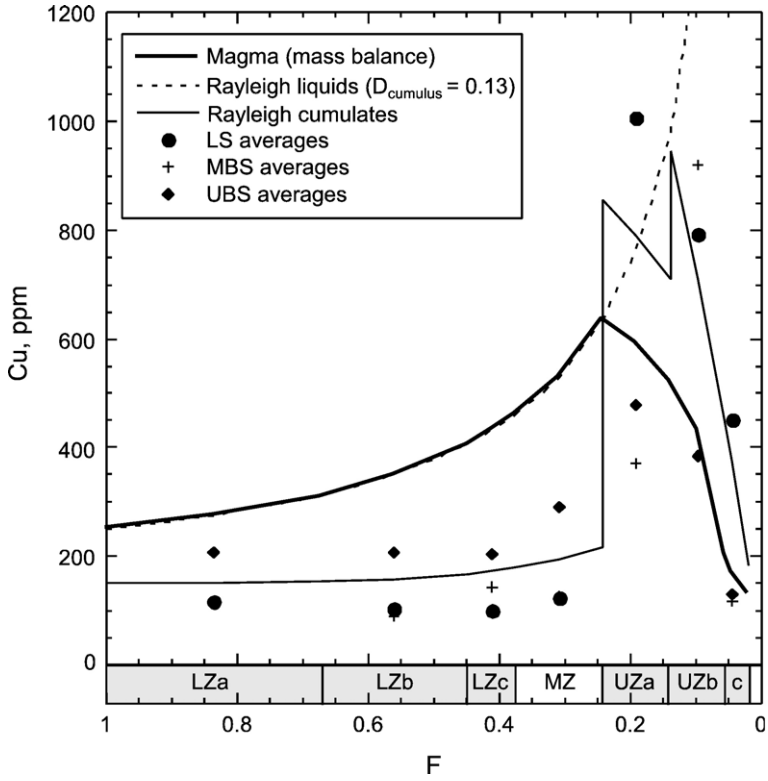

Fig. 8. Variations in the Cu-concentrations as a function of the fraction of liquid remaining (F). Prior to sulphur saturation, the magma evolution, as determined by mass balance (solid line) matches closely to an incompatible fractionation curve with a $D^{Cu}_{cumulus}=0.13$. The evolution after sulphur saturation can be roughly fitted to a $D^{Cu}_{cumulus}=1.4$ through UZa and $D^{Cu}_{cumulus}=1.9$ through UZb and UZc. Average LS, MBS, and UBS concentrations from McBirney (1989a), with MZ modified following data from McBirney (1998). Data are presented in Tables 3 and 5.

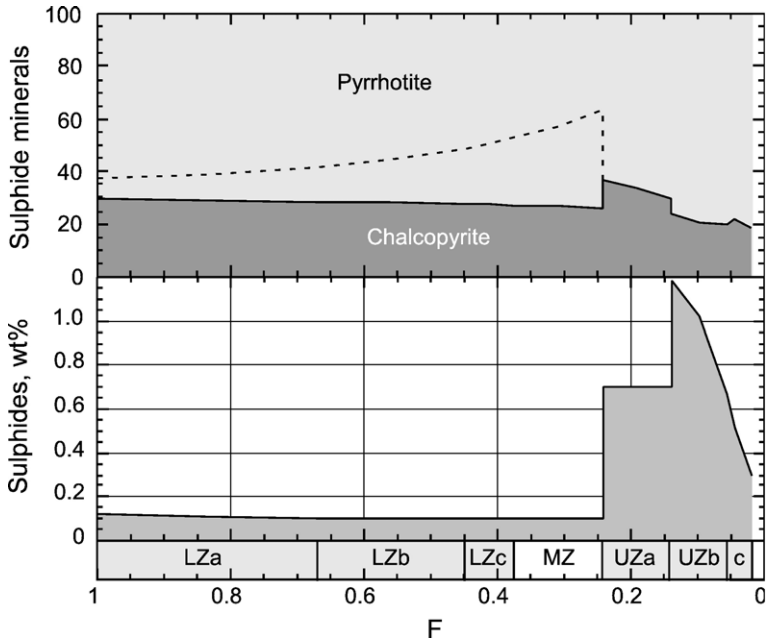

Fig. 9. Relative and absolute abundance of sulphide minerals in the LS. Relative abundances are modeled at liquidus and after complete reequilibration of Cu (dashed line). Data are presented in Table 6.

chalcopyrite, and the remaining sulphur balanced by Fe^{2+} and form pyrrhotite, the model yields 0.10 wt.% (0.07 modal %) sulphides throughout LZ and MZ. The weight proportion of chalcopyrite/pyrrhotite evolves from 30:70 at the base of LZa to 26:74 in the upper part of MZ (Table 6 and Fig. 9).

The rate of sulphur fractionation in UZ has been estimated by matching Eq. (8) to the slope of the sulphur saturation curve in Fig. 7. A reasonable fit is achieved (by iteration) at a $D^{S}_{cumulus}=0.99$ through UZa and a $D^{S}_{cumulus}=0.74$ through UZb. This gives (by using Eq. (9)) an expected sulphur concentration in the cumulate of 2584 ppm at the MZ–UZa boundary. For Cu, a similar fit to the mass balance curve (Fig. 8) can be achieved at $D^{Cu}_{cumulus}=1.4$ through UZa and $D^{Cu}_{cumulus}=1.9$ through UZb (again by iteration). This gives 854 ppm Cu in the cumulate at the MZ–UZ boundary. These values correspond to 0.70 wt.% (0.53 modal %) sulphides. The apparent changes in partition coefficients at the base of UZb are artifacts of the very mafic composition of this unit. As such, the relative values derived from the mass balance are comparable, but no great emphasis can be placed on their absolute values. However, it is significant that Cu is taken out at a greater rate than S, which implies an evolution towards more pyrrhotite-rich compositions during fractionation. The modeling yields 0.30 to 1.18 wt.% (0.19 to 0.89 modal %) sulphides through the UZ (Table 7 and Fig. 9). The weight proportion of chalcopyrite/pyrrhotite evolves from 35:65 at the base of UZa to 18:82 at the SH.

5.3. Sulphur saturation induced by contamination

Calculations on the effect of contamination of the LZa parental magma yield sulphur saturation only by the addition of substantial amounts of contaminant (Table 7 and Fig. 10). At the dry LZa liquidus, more than 22 wt.% contamination is required with a contaminant having 1000 ppm S, more than 28 wt.% at 500 ppm, more than 33 wt.% at 200 ppm, and more than 40 wt.% at 50 ppm or less. Localised temperature reduction will significantly reduce these

Table 7
The effect of contamination with leucogranophyre on the LZa parental magma

	Contaminant	LZa parental magma	Degree of contamination				
			10 wt.%	20 wt.%	30 wt.%	40 wt.%	50 wt.%
SiO_2	75.03	47.51	50.26	53.01	55.76	58.52	61.27
TiO_2	0.31	2.98	2.71	2.45	2.18	1.91	1.65
Al_2O_3	13.17	13.35	13.33	13.32	13.30	13.28	13.26
FeO	1.98	15.61	14.24	12.88	11.52	10.16	8.80
MnO	0.01	0.23	0.21	0.18	0.16	0.14	0.12
MgO	0.15	7.08	6.39	5.70	5.00	4.31	3.62
CaO	0.69	9.84	8.92	8.01	7.09	6.18	5.26
Na_2O	4.24	2.48	2.66	2.83	3.01	3.18	3.36
K_2O	3.85	0.39	0.74	1.08	1.43	1.77	2.12
P_2O_5	0.03	0.27	0.25	0.22	0.20	0.18	0.15
Total	99.47	99.73	99.71	99.68	99.65	99.63	99.60
$\log X^{FeO}$	−1.7451	−0.8608	−0.8993	−0.9418	−0.9892	−1.0427	−1.1040
$\log X^{S}$ at							
$C^{S}=0$ ppm		−2.7523	−2.7969	−2.8469	−2.9037	−2.9695	−3.0476
$C^{S}=5$ ppm	−4.9931	−2.7523	−2.7966	−2.8463	−2.9027	−2.9679	−3.0451
$C^{S}=10$ ppm	−4.6921	−2.7523	−2.7964	−2.8457	−2.9017	−2.9663	−3.0427
$C^{S}=20$ ppm	−4.3911	−2.7523	−2.7958	−2.8445	−2.8996	−2.9631	−3.0380
$C^{S}=50$ ppm	−3.9931	−2.7523	−2.7942	−2.8409	−2.8935	−2.9536	−3.0239
$C^{S}=100$ ppm	−3.6921	−2.7523	−2.7915	−2.8349	−2.8834	−2.9383	−3.0015
$C^{S}=200$ ppm	−3.3911	−2.7523	−2.7862	−2.8233	−2.8640	−2.9092	−2.9599
$C^{S}=500$ ppm	−2.9931	−2.7523	−2.7707	−2.7901	−2.8104	−2.8319	−2.8547
$C^{S}=1000$ ppm	−2.6921	−2.7523	−2.7460	−2.7398	−2.7337	−2.7276	−2.7216
$\log X^{S}$ (saturation) at							
T_L	−5.9931	−2.5524	−2.6358	−2.7293	−2.8362	−2.9610	−3.1119
T_L-10 K	<6	−2.5617	−2.6471	−2.7435	−2.8544	−2.9855	−3.1471
T_L-50 K	<6	−2.6010	−2.6956	−2.8050	−2.9359	−3.1002	−3.3260
T_L-100 K	<6	−2.6558	−2.7649	−2.8968	−3.0655	−3.3062	−3.7662

Sulphur saturation is calculated for different concentrations in the contaminant magma ($C^{S}=0$–1000 ppm) at the LZa liquidus temperature (T_L) as well as 10, 50, and 100 K below.

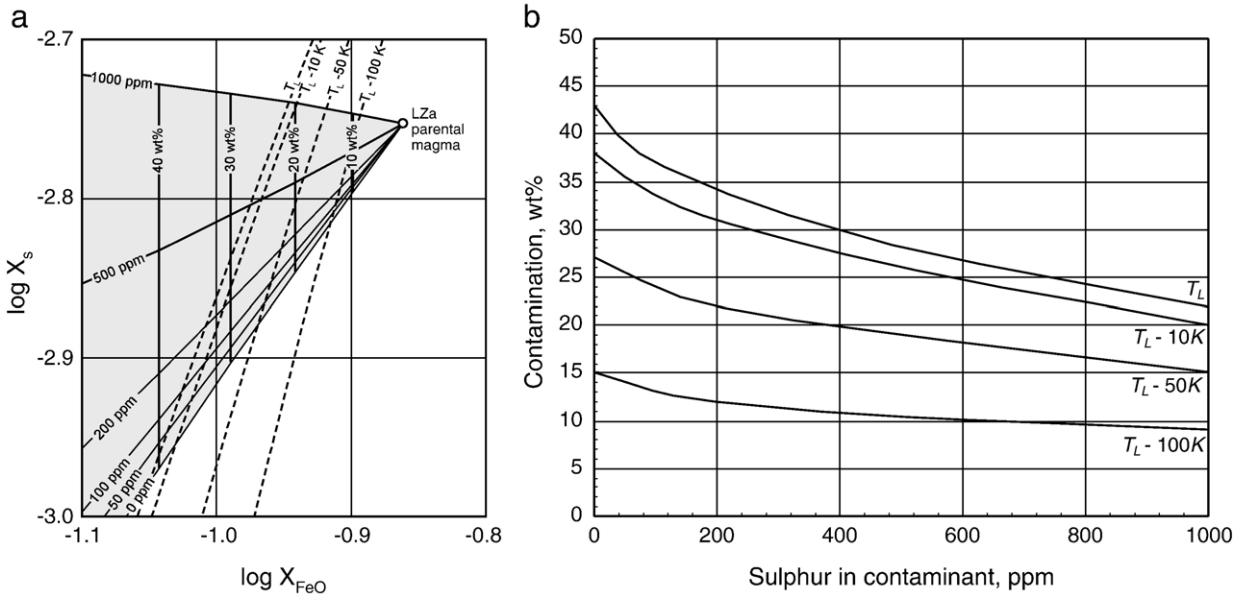

Fig. 10. The effect of contamination on the sulphur saturation of the LZa parental magma. (a) Diagram showing the effect of contamination (values in wt.%) with granophyre having different concentrations of sulphur (values in ppm) on the LZa parental magma. Saturation curves (dashed) are included for the LZa liquidus temperature (T_L), as well as 10 K, 50 K, and 100 K below. Diagram following Poulson and Ohmoto (1990). (b) Diagram showing the extent of contamination required to produce sulphur saturation for contaminants with different sulphur contents (extracted visually from a). Data are presented in Table 7.

values, a 100 K reduction to less than half of the values required at the liquidus.

6. Discussion

6.1. Sulphur saturation and magmatic differentiation

The Rayleigh fractionation of sulphur up through LZa and LZb yields a trend that is unsaturated and broadly parallel to the saturation curve (Fig. 7). Although the FeO content of the magma continues to increase through LZc and MZ (Fig. 4), the onset of titanomagnetite crystallisation in LZc changes the Rayleigh fractionation trend to approach the saturation curve. The saturation curve is reached in the upper part of MZ causing the formation of sulphide liquid. This highlights the potential significance of iron–titanium oxide crystallisation for sulphur saturation and the formation of late-stage PGE reefs in layered intrusions (cf., Prendergast, 2000; Maier et al., 2003).

6.2. Primary sulphide mineralogy of the Skaergaard Intrusion

Sulphide minerals of the Skaergaard Intrusion are dominated by bornite, digenite, and chalcocite (Andersen et al., 1998; Nielsen et al., 2003a,b,c,d,e). This paragenesis is quite different to the compositions resulting from the modeling above. Although high-temperature forms of bornite and digenite have been reported at magmatic temperatures (e.g., Karup-Møller and Makovicky, 1999; Ripley et al., 2002), they have not been synthesized from natural basaltic magmas. Nielsen et al. (2003a,b,c,d,e) argued that sulphide minerals largely preserve their interstitial and, in places droplike, shapes, which they interpreted as evidence for their primary magmatic origin. However, it is clear from the modeling presented here, that the current mineral assemblages cannot accommodate the amount of sulphur required for saturation to have occurred. The textural evidence is intriguing and requires further studies, but based on present evidence, it must be inferred that the sulphides are subsolidus mineral assemblages. As such, they are unlikely to have preserved primary magmatic textures or evidence for alteration and reequilibration. The modeling presented here shows, that unless current models for sulphur saturation are inappropriate, the Skaergaard sulphides must have been significantly modified after their primary deposition from a sulphide liquid.

During the sulphur unsaturated LZ and MZ fractionation, the modeled Cu concentrations of the cumulate rocks fall close to the weighted averages of the lithological units (Fig. 8), but S concentrations are systematically lower than the modeled values (Fig. 7), which indicates significant loss of sulphur. Partition

coefficients indicate significant incorporation of Cu into the cumulus silicate minerals. Considering the relatively constant partition coefficient throughout, the most likely mineral host is augite. The modeling indicates that approximately 20% of the Cu is likely to have been retained in the primary cumulus minerals in LZa and as much as 60% in the upper part of MZ prior to sulphur saturation. The remaining Cu and all of the S reside in the trapped interstitial liquid and would be expected to form trace amounts of discrete sulphide minerals.

Because of the low abundance of sulphides (0.10 wt.%) in the LZ and MZ, it is possible that they have been significantly modified by reequilibration of Cu. The generally unzoned compositions of olivine and pyroxenes, as well as the extensive postcumulus exsolutions in the pyroxenes (cf., Nobugai et al., 1978; Nakajima and Hafner, 1980), show that these minerals underwent significant postcumulus modification. Therefore, reequilibration of Cu is likely. A complete reequilibration of Cu into sulphides combined with a conversion of chalcopyrite and pyrrhotite to bornite and magnetite would reduce the sulphur to 14.3 % of the original concentration at the base of LZa, and 24.7% in the upper part of MZ (Table 5 and Fig. 7).

After sulphur-saturation, because of the higher sulphide content (0.70 wt.%), more than 90% of the Cu as well as all of the S is expected to reside in the sulphide minerals. Consequently reequilibration with mafic silicate minerals can only have had negligible effect on the sulphide composition, and the present digenite–bornite–chalcopyrite assemblage would be likely to have been derived largely by sulphur loss. A complete conversion of pyrrhotite and chalcopyrite to magnetite and bornite during oxidation would reduce the sulphur to between 13.3% (in UZa) and 6.7% (in UZc) of the original concentrations (Table 5 and Fig. 7), which roughly concords with the lower limit of present-day concentrations (400–900 ppm, Turner, 1986).

6.3. Copper or sulphur saturation during closed system magmatic differentiation

The most obvious result of this exercise is, that at present there is far too little sulphur available in the Skaergaard Intrusion to explain sulphur saturation at the Platinova Reef following current models. This implies either that other factors (such as, for example, the contents of metals) were important for the formation of sulphide liquids, or that the original sulphur content has been significantly reduced by later processes.

An interesting possibility is whether liquid immiscibility could have been triggered by Cu and noble metal rather than S saturation (following the suggestions for the existence of a separate alloy liquid by Bird et al., 1991). The modeled Cu concentration at the MZ–UZa boundary does actually exceed the lower limit for saturation in a S-poor basaltic system (Ripley et al., 2002). However, there is no field or experimental evidence to support the formation of Cu–alloy liquids from natural magmas. Similarly, considering the solubilities of noble metals in basaltic magmas (Borisov and Palme, 1996, 1997, 2000) and sulphide liquids (Makovicky et al., 1986, 1995), it is unlikely that a separate noble metal liquid can exist at the sulphide liquidus. In contrast, it would appear more reasonable for Cu and noble metals to combine with the sulphide rather than form a separate alloy liquid.

6.4. Postmagmatic sulphur mobility and redistribution

The formation of Cu-rich, Fe-poor sulphides through postmagmatic oxidation and sulphur-loss has previously been described from intrusions in the Okiep district, South Africa (Cawthorn and Meyer, 1993) and the Curaçá Valley, Brazil (Maier and Barnes, 1996). As shown above, for the Skaergaard Intrusion, the sulphur saturation model would require an initial sulphide mineral assemblage with approximately 82% Fe-rich MSS (pyrrhotite) and 18% ISS (chalcopyrite). The present-day sulphur concentrations and sulphide mineralogy require extensive loss of sulphur to have occurred after the formation of the sulphides. Oxidation is expected to attack sulphides and mobilise sulphur as H_2S or SO_2. The consequence would be a conversion of pyrrhotite to Fe-oxides, and chalcopyrite to Fe-oxides and bornite, digenite, chalcocite, and under extreme circumstances native Cu. Such a model is in accord with the observed association between bornite and Ti-poor magnetite (Andersen et al., 1998).

Seen in light of the extensive signs of oxidation and hydrothermal activity in the Skaergaard Intrusion (Buddington and Lindsley, 1964; Norton and Taylor, 1979; Taylor and Forester, 1979; Bird et al., 1986), it is not surprising if the sulphides have been altered. Signs of oxidation are particularly well expressed in the extensive oxidation exsolution textures of titanomagnetite. Thermodynamic calculations reveal equilibration temperatures down to 540 °C in the Platinova Reef (Andersen, 1996). Furthermore, oxygen isotopes show extensive exchange of oxygen with meteoric water in the upper half of the intrusion (Taylor and Forester, 1979). Also particularly significant for the Platinova Reef, the Re–Os isotopic system has been disturbed (Brooks et al., 1999) – possibly as a result of Re-mobilisation. This indicates that Pd and Au could also potentially have been affected by the mobilisation.

The following processes can adequately explain the evolution of sulphides displayed through the Skaergaard Layered Series:

LZa–UZb (digenite–bornite–chalcopyrite–magnetite): There is evidence for significant sulphur loss from most of the LS. This sulphur loss is best explained in the context of oxidation. Likely reactions are:

$$15CuFeS_2 + 26O_2 \leftrightarrow 3Cu_5FeS_4 + 4Fe_3O_4 + 18SO_2 \quad (14)$$

chalcopyrite + oxygen↔bornite + magnetite + SO_2

$$3Fe_{1-x}S + (5-2x)O_2 \leftrightarrow (1-x)Fe_3O_4 + 3SO_2 \quad (15)$$

pyrrhotite + oxygen↔magnetite + SO_2

Some reequilibration of Cu from cumulus silicates into sulphides could have occurred in rocks formed prior to sulphur saturation as their sulphide contents are low. Possible reequilibration reactions are:

$$3CuFeS_2 + 2Cu^{2+} + 2O_2 \leftrightarrow Cu_5FeS_4 + 2Fe^{2+} + 2SO_2 \quad (16)$$

chalcopyrite + Cu (in augite) + oxygen↔bornite + Fe (in augite) + SO_2

$$4Fe_{1-x}S + 5Cu^{2+} \leftrightarrow Cu_5FeS_4 + (3-4x)\ Fe^{2+} \quad (17)$$

pyrrhotite + Cu (in augite)↔bornite + Fe (in augite)

UZc (pyrrhotite–chalcopyrite–marcasite): The different mineralogy in UZc can be explained with an addition of sulphur sourced by oxidation of sulphides in the lower cumulates. This can be explained by the following reaction:

$$Fe_{1-x}S + (1-2x)\ SO_2 \leftrightarrow (1-x)\ FeS_2 + (1-2x)\ O_2 \quad (18)$$

pyrrhotite + SO_2↔marcasite + oxygen.

6.5. Structure of the Platinova Reef

The structure of the Platinova Reef could potentially have been influenced by mobilisation of sulphur. The intricate internal structure of successive Pd-rich strata within the stratabound reef appears to be intimately linked to the magmatic layering, although the factors controlling the metal concentration are unclear. As the individual strata are perfectly concordant with the modal layering, it is likely that they are controlled by the primary mineralogical variations.

The variable, but systematic separation of Pd and Au across the reef can be explained in the context of oxidation and sulphur mobilisation. The most likely agents for sulphur transport could be late-magmatic or hydrothermal fluids migrating upwards through the reef. A fluid, possibly initially Cl-rich, could be able to dissolve and transport Pd and Au from an initially stratiform Platinova Reef (cf. Boudreau and Meurer, 1999). The first occurrence of cumulus Cu–Fe sulphides would likely act as a significant redox barrier, and upward migrating fluids would respond by assimilating sulphur. This would be expected to lead to a change in their pH and redox potential, thereby

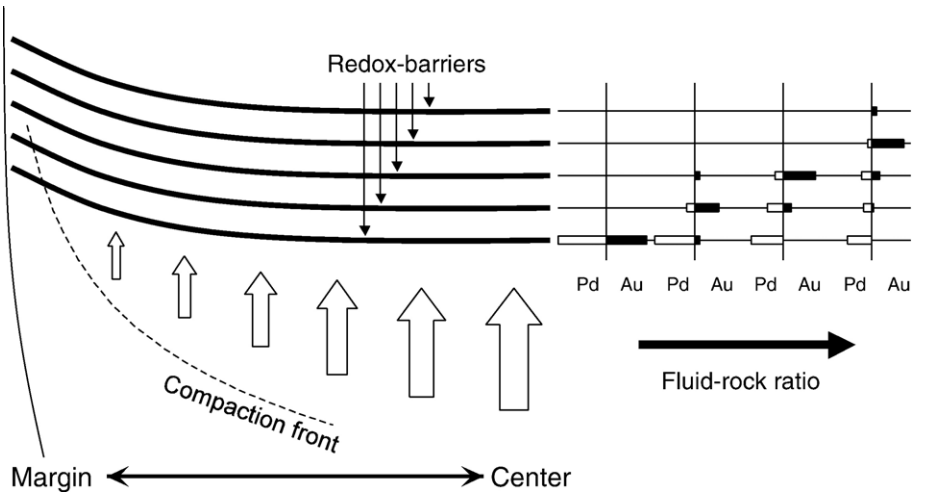

Fig. 11. Schematic illustration (not to scale) of the potential effect of sulphur-loss on a stratiform occurrence of Pd and Au during upward deuteric or hydrothermal fluid migration in a cumulate with successive stratabound redox barriers (e.g. sulphide- or oxide-rich strata). The relative volumes of fluids are indicated from the margin towards the centre of the intrusion by the sizes of the block arrows. The relative effects of fluid mobilisation and reprecipitation of Pd and Au are illustrated to the right.

influencing their capacity for carrying PGE (Mountain and Wood, 1987; Wood, 1987, 2002). An addition of H_2S or SO_2 to the fluid could keep Au mobile as the relatively soluble $Au(HS)_2^-$. In contrast, Pd would be expected to be retained in the rocks, as the solubility of the equivalent Pd-species (most likely $Pd(HS)_2^0$) is much smaller (Wood, 2002). Successive re-precipitation and re-dissolution of Pd and Au would be expected to occur in overlying oxide- or sulphide-bearing strata as the sulphur is progressively depleted from below (Fig. 11).

Migration of late-magmatic interstitial fluids is essentially controlled by compaction of the LS cumulates and it would be expected to be largest in the centre of the intrusion where the compaction will be greatest. Similarly, as a consequence of the heat-driven hydrothermal convection (Norton and Taylor, 1979), hydrothermal fluids would also be expected to show the greatest mobility near the centre of the intrusion. In the light of a pre-existing stratification, both processes would therefore adequately explain the largest separation of Au and Pd in the centre of the intrusion as well as the overall discordance of the Au-horizon (cf., Nielsen, 2001).

6.6. Contamination and composition of the chilled margin

The relatively large amount of contaminant required for the LZa parental magma to yield sulphur saturation indicates that contamination-related sulphides would only be expected in very few places in the Skaergaard Intrusion. There is no field evidence to suggest that the bulk composition of the Skaergaard magma was significantly affected by contamination. Stewart and DePaolo (1990) calculated 2–4% overall contamination of the Skaergaard magma by Precambrian gneiss from Nd and Sr isotopes. This is far below the contamination required for sulphides to form (Fig. 10). Although they suggested that the Skaergaard magma could have been capped by significant amounts of granophyre, there is no field evidence from the UBS (Naslund, 1984) or the abundant fallen blocks (Irvine et al., 1998) to support this hypothesis. Large amounts of contamination, and associated sulphide fractionation, is only feasible locally where xenoliths have been partially fused and mixed with the magma in the outer parts of the MBS (as observed on Mellemø).

Sulphur saturation by contamination in the MBS could have significantly influenced the distribution of sulphur and chalcophile elements. Bearing in mind the inhomogeneity of the chilled margin (Hoover, 1989a), the abundance of partially digested xenoliths, and the presence of sulphide-rich patches in the outer parts of the MBS, it is likely that the distribution of chalcophile and noble metals has been significantly disturbed. This could partly explain the highly heterogeneous distribution of S, Cu, Co, Pd, and Au in the chilled margin and outer parts of the MBS (cf., Goles et al., 1974; Andersen et al., 1998; Nielsen, 2001). However, because the outer parts of the MBS are expected to have crystallised before the onset of magma convection (Wager and Deer, 1939; Hoover, 1989a), this fractionation probably took place without much elemental interchange with the main magma body. Consequently, the effect on the general fractionation was likely to be negligible.

7. Conclusions

- The parental magma to LZa contained around 250 ppm Cu and 894 ppm S. Sulphur saturation was reached in the upper part of MZ at concentrations around 635 ppm Cu and 2607 ppm S.
- The primary sulphide assemblage evolved from 30 wt.% chalcopyrite and 70 wt.% pyrrhotite at the base of LZa to 18 wt.% chalcopyrite and 82 wt.% pyrrhotite in UZc.
- The LZ and MZ contained around 0.07 modal % primary sulphides.
- The UZ contained on average 0.53 modal % primary sulphides.
- During LZ and MZ fractionation, Cu was extensively incorporated into mafic cumulus phases (most likely augite). Reequilibration of Cu into interstitial sulphides can partially explain their present Cu-rich compositions.
- The lower parts of the LS (from LZa to UZb) experienced extensive sulphur-loss during postmagmatic oxidation. A sulphur-gain in UZc can possibly explain the occurrence of marcasite and the high S concentrations reported by Wager et al. (1957).
- Apart from the MBS (and the chilled margin), contamination is unlikely to have had any major effect on the sulphur fractionation in the intrusion.

8. Notations used

C_0	Initial concentration
C_S	Concentration, phases in subscript (L = liquid, S = solid), elements in superscripts (S = sulphur, Cu = copper)
D	Bulk solid/liquid partition coefficient, elements in superscript

$D_{cumulus}$ Bulk solid/liquid partition coefficient for cumulus material (excluding the trapped liquid), elements in superscript
F Fraction of liquid remaining
$K_{D,i}$ Mineral–melt partition coefficient for mineral i
log Logarithm (base 10)
P Pressure (bar)
T Temperature (K)
T_L Liquidus temperature
w_i Weight fraction of mineral or component i
W_{TL} Weight fraction (percent where stated) of trapped liquid
X Molar fraction, elements or components in superscript.

Acknowledgments

This paper honours the contributions of Kent Brooks to the geological exploration of the Palaeogene igneous activity on East Greenland. Kent has been an invaluable source of inspiration and enthusiasm, funding, organisation, and field support to the author throughout his career. The author likes to thank Stefan Bernstein and Christian Tegner for organising the June 2–5 2004 symposium at Brorfelde (Denmark) and this volume. Constructive discussions with Kent Brooks, Neil Irvine, Troels Nielsen, and Nigel Powell; and thorough reviews by Grant Cawthorn, Christian Tegner and one anonymous reviewer are appreciated.

References

Andersen, J.C.Ø., 1996. The Skaergaard Intrusion and the Platinova gold and palladium deposit, Kangerlussuaq area, East Greenland. PhD thesis, Copenhagen University.

Andersen, J.C.Ø., Rasmussen, H., Nielsen, T.F.D., Rønsbo, J.G., 1998. The Triple Group and the Platinova gold and palladium reefs in the Skaergaard Intrusion: stratigraphic and petrographic relations. Economic Geology 93, 488–509.

Andersen, J.C.Ø., Power, M.R., Momme, P., 2002. Platinum-group elements in the Palaeogene North Atlantic Igneous Province. In: Cabri, L.J. (Ed.), The Geology, Geochemistry, Mineralogy, and Mineral Beneficiation of Platinum-Group Elements, vol. 54. Canadian Institute of Mining, Metallurgy, and Petroleum. CIM Special Volume, Montréal, Québec, pp. 637–667. ISBN 1-894475-27-5.

Bird, D.K., Rogers, R.D., Manning, C.E., 1986. Mineralized fracture systems of the Skaergaard Intrusion, East Greenland. Meddelelser om Grønland. Geoscience 16, 1–65.

Bird, D.K., Brooks, C.K., Gannicott, R.A., Turner, P.A., 1991. A gold-bearing horizon in the Skaergaard Intrusion, East Greenland. Economic Geology 86, 1083–1092.

Bird, D.K., Arnason, J.G., Brandriss, M.E., Nevle, R.J., Radford, G., Bernstein, S., Gannicott, R.A., Kelemen, P.B., 1995. A gold-bearing horizon in the Kap Edvard Holm Complex, East Greenland. Economic Geology 90, 1288–1300.

Blank, H.R., Gettings, M.E., 1973. Subsurface form and extent of the Skaergaard Intrusion, East Greenland. EOS, Transactions-American Geophysical Union 54, 507.

Borisov, A., Palme, H., 1996. Experimental determination of the solubility of Au in silicate melts. Mineralogy and Petrology 56, 297–312.

Borisov, A., Palme, H., 1997. Experimental determination of the solubility of platinum in silicate melts. Geochimica et Cosmochimica Acta 61, 4349–4357.

Borisov, A., Palme, H., 2000. Solubilities of noble metals in Fe-containing silicate melts as derived from experiments in Fe-free systems. American Mineralogist 85, 1665–1673.

Boudreau, A.E., Meurer, W.P., 1999. Chromatographic separation of the platinum-group elements, gold, base metals and sulfur during degassing of a compacting and solidifying igneous crystal pile. Contributions to Mineralogy and Petrology 134, 174–185.

Bowen, N.L., 1928. The Evolution of the Igneous Rocks. Princeton University Press, Princeton. 332 pp.

Brooks, C.K., Gleadow, A.J.W., 1977. A fission-track age for the Skaergaard Intrusion and the age of East Greenland basalts. Geology 5, 539–540.

Brooks, C.K., Nielsen, T.F.D., 1978. Early stages in the differentiation of the Skaergaard magma as revealed by a closely related suite of dike rocks. Lithos 11, 1–14.

Brooks, C.K., Larsen, L.M., Nielsen, T.F.D., 1991. Importance of iron-rich tholeiitic magmas at divergent plate margins: a reappraisal. Geology 19, 269–272.

Brooks, C.K., Keays, R.R., Lambert, D.D., Frick, L.R., Nielsen, T.F.D., 1999. Re–Os isotope geochemistry of Tertiary picritic and basaltic magmatism of East Greenland: constraints on plume–lithosphere interactions and the genesis of the Platinova Reef, Skaergaard Intrusion. Lithos 47, 107–126.

Buddington, A.F., Lindsley, D.H., 1964. Iron–titanium oxide minerals and their synthetic equivalents. Journal of Petrology 5, 310–357.

Butcher, A.R., Pirrie, D., Prichard, H.M., Fisher, P., 1999. Platinum-group mineralization in the Rum layered Intrusion, Scottish Hebrides, UK. Journal of the Geological Society 156, 213–216.

Cawthorn, R.G., Meyer, F.M., 1993. Petrochemistry of the Okiep copper district basic intrusive bodies, Northwestern Cape Province, South Africa. Economic Geology 88, 590–605.

Cawthorn, R.G., Walsh, K.L., 1988. The use of phosphorus contents in yielding estimates of the proportion of trapped liquid in cumulates of the Upper Zone of the Bushveld Complex. Mineralogical Magazine 52, 81–89.

Chayes, F., 1970. On estimating the magnitude of the Hidden Zone and the compositions of the residual liquids of the Skaergaard Layered Series. Journal of Petrology 11, 1–14.

Chayes, F., 1971. Ratio Correlation: A Manual for Students of Petrology and Geochemistry. University of Chicago Press, Chicago. 99 pp.

Gaetani, G.A., Grove, T.L., 1997. Partitioning of moderately siderophile elements among olivine, silicate melt, and sulfide melt: constraints on core formation in the Earth and Mars. Geochimica et Cosmochimica Acta 61, 1829–1846.

Ghiorso, M.S., Sack, R.O., 1995. Chemical mass-transfer in magmatic processes: 4. A revised and internally consistent thermodynamic model for the interpolation and extrapolation of liquid–solid equilibria in magmatic systems at elevated temperatures and pressures. Contributions to Mineralogy and Petrology 119, 197–212.

Goles, G.G., Hering, C., Vincent, E.A., 1974. Evolution of Co, Sc and Cr abundances in the Skaergaard magmatic liquids. EOS, Transactions-American Geophysical Union 55, 459.

Haughton, D.R., Roeder, P.L., Skinner, B.J., 1974. Solubility of sulfur in mafic magmas. Economic Geology 69, 451–467.

Henderson, P., 1982. Inorganic Geochemistry. Pergamon Press, Oxford. 353 pp.

Hirschmann, M.M., Renne, P.R., McBirney, A.R., 1997. $^{40}Ar/^{39}Ar$ dating of the Skaergaard Intrusion. Earth and Planetary Science Letters 146, 645–658.

Holzheid, A., Lodders, K., 2001. Solubility of copper in silicate melts as function of oxygen and sulfur fugacities, temperature, and silicate composition. Geochimica et Cosmochimica Acta 65, 1933–1951.

Hoover, J.D., 1989a. The chilled marginal gabbro and other contact rocks of the Skaergaard Intrusion. Journal of Petrology 30, 441–476.

Hoover, J.D., 1989b. Petrology of the marginal border series of the Skaergaard Intrusion. Journal of Petrology 30, 399–439.

Hulbert, L.J., Duke, J.M., Ekstrand, O.R., Scoates, R.F.J., Theriault, R. J., LeCheminant, M.J., Gunn, A.G., Grinenko, L.N., 1992. Metallogenic and geochemical evolution of cyclic Unit 1, lower Eastern Layered Series, Rhum. In: Foster, R.P. (Ed.), Mineral Deposit Modelling in Relation to Crustal Reservoirs of Ore-Forming Elements. Institute of Mining and Metallurgy, London.

Hunter, R.H., Sparks, R.S.J., 1987. The differentiation of the Skaergaard Intrusion. Contributions to Mineralogy and Petrology 95, 451–461.

Irvine, T.N., Andersen, J.C.Ø., Brooks, C.K., 1998. Included blocks (and blocks within blocks) in the Skaergaard Intrusion: geological relations and the origins of rhythmic modally graded layers. Geological Society of America Bulletin 110, 1398–1447.

Karup-Møller, S., Makovicky, E., 1999. The phase system Cu–Pd–S at 900 degrees, 725 degrees, 550 degrees, and 400 degrees C. Neues Jahrbuch für Mineralogie Monatshefte 1999, 551–567.

Larsen, R.B., Tegner, C., 2006. Pressure conditions for the solidification of the Skaergaard Intrusion: eruption of East Greenland flood basalts in less than 300.000 years. Lithos (this volume).

Larsen, L.M., Watt, W.S., Watt, M., 1989. Geology and petrology of the Lower Tertiary plateau basalts of the Scoresby Sund region, East Greenland. Bulletin of the Greenland Geological Survey 157 (164 pp.).

Li, C., Maier, W.D., de Waal, S.A., 2001. The role of magma mixing in the genesis of the PGE mineralization in the Bushveld Complex: thermodynamic calculations and new interpretations. Economic Geology 96, 653–662.

Lindsley, D.H., Brown, G.M., Muir, I.D., 1969. Conditions of the ferrowollastonite–ferohedenbergite inversion in the Skaergaard Intrusion, East Greenland. Special Paper-Mineralogical Society of America 2, 193–201.

Maier, W.D., Barnes, S.-J., 1996. Unusually high concentrations of magnetite at Caraíba and other Cu-sulfide deposits in the Curaçá valley, Bahia, Brazil. Canadian Mineralogist 34, 717–731.

Maier, W.D., Barnes, S.-J., Gartz, V., Andrews, G., 2003. Pt–Pd reefs in magnetities of the Stella layered intrusion, South Africa: a world of new exploration opportunities for platinum group elements. Geology 31, 885–888.

Makovicky, M., Makovicky, E., Rose-Hansen, J., 1986. Experimental studies on the solubility and distribution of platinum group elements in base-metal sulphides in platinum deposits. In: Gallagher, M.J., Ixer, R.A., Neary, C.R., Prichard, H.M. (Eds.), Metallogeny of Basic and Ultrabasic Rocks. The Institution of Mining and Metallurgy, London, pp. 415–425.

Makovicky, M., Makovicky, E., Rose-Hansen, J., Barnes, S.-J., 1995. Skaergaard Intrusion in a test tube – current results. In: Pasava, J., Kribek, B., Zak, K. (Eds.), Mineral Deposits. Rotterdam, Balkema, pp. 145–147.

Mavrogenes, J.A., O'Neill, H.S.C., 1999. The relative effects of pressure, temperature and oxygen fugacity on the solubility of sulfide in mafic magmas. Geochimica et Cosmochimica Acta 63, 1173–1180.

McBirney, A.R., 1975. Differentiation of the Skaergaard Intrusion. Nature 253, 691–694.

McBirney, A.R., 1989a. The Skaergaard Layered Series: I. Structure and average composition. Journal of Petrology 30, 363–397.

McBirney, A.R., 1989b. Geological Map of the Skaergaard Intrusion, East Greenland, 1 : 20 000. University of Oregon, Eugene, Oregon.

McBirney, A.R., 1998. The Skaergaard Layered Series: Part V. Included trace elements. Journal of Petrology 39, 255–276.

Miller Jr., J.D., 1999. Geochemical evaluation of platinum group element (PGE) mineralization in the Sonju Lake Intrusion, Finland, Minnesota. Information Circular-Minnesota Geological Survey 44 .32 pp.

Miller Jr., J.D., Andersen, J.C.Ø., 2002. Attributes of Skaergaard-type PGE reefs. In: Boudreau, A.E. (Ed.), 9th International Platinum Symposium Abstracts, pp. 305–308.

Momme, P., Tegner, C., Brooks, C.K., Keays, R.R., 2002. The behaviour of platinum-group elements in basalts from the East Greenland rifted margin. Contributions to Mineralogy and Petrology 143, 133–153.

Morse, S.A., Lindsley, D.H., Williams, R.J., 1980. Concerning intensive parameters in the Skaergaard Intrusion. American Journal of Science 280A, 159–170.

Mountain, B.W., Wood, S.A., 1987. Solubility and transport of platinum-group elements in hydrothermal solutions: thermodynamic and physical chemical constraints. In: Prichard, H.M., Potts, P.J., Bowles, J.F.W., Cribb, S.J. (Eds.), Geo-Platinum, vol. 87. Elsevier Applied Science, London, pp. 57–82.

Nakajima, Y., Hafner, S.S., 1980. Exsolution in augite from the Skaergaard Intrusion. Contributions to Mineralogy and Petrology 72, 101–110.

Naslund, H.R., 1984. Petrology of the Upper Border Series of the Skaergaard Intrusion, East Greenland. Journal of Petrology 25, 185–212.

Nielsen, T.F.D., 2001. The palladium potential of the Skaergaard Intrusion, South-East Greenland. Danmarks og Grønlands Geologiske Undersøgelse Rapport 2001/23. 39 pp.

Nielsen, T.F.D., 2004. The shape and volume of the Skaergaard Intrusion, Greenland: implications for mass balance and bulk composition. Journal of Petrology 45, 507–530.

Nielsen, T.F.D., Rasmussen, H., Rudashevsky, N.S., Kretser, Yu.L., Rudashevsky, V.N., 2003a. PGE and sulphide phases of the precious metal mineralisation of the Skaergaard Intrusion: Part 1. Sample 90-23A, 807. Danmarks og Grønlands Geologiske Undersøgelse Rapport 2003/47, 1–20.

Nielsen, T.F.D., Rasmussen, H., Rudashevsky, N.S., Kretser, Yu.L., Rudashevsky, V.N., 2003b. PGE and sulphide phases of the precious metal mineralisation of the Skaergaard Intrusion: Part 2. Sample 90-24, 1057. Danmarks og Grønlands Geologiske Undersøgelse Rapport 2003/48, 1–20.

Nielsen, T.F.D., Rasmussen, H., Rudashevsky, N.S., Kretser, Yu.L., Rudashevsky, V.N., 2003c. PGE and sulphide phases of the precious metal mineralisation of the Skaergaard Intrusion: Part 3. Sample 90-18, 1010. Danmarks og Grønlands Geologiske Undersøgelse Rapport 2003/52, 1–25.

Nielsen, T.F.D., Rasmussen, H., Rudashevsky, N.S., Kretser, Yu.L., Rudashevsky, V.N., 2003d. PGE and sulphide phases of the

precious metal mineralisation of the Skaergaard Intrusion: Part 4. Sample 90-23A, 806. Danmarks og Grønlands Geologiske Undersøgelse Rapport 2003/53, 1–18.

Nielsen, T.F.D., Rasmussen, H., Rudashevsky, N.S., Kretser, Yu.L., Rudashevsky, V.N., 2003e. PGE and sulphide phases of the precious metal mineralisation of the Skaergaard Intrusion: Part 5. Sample 90-23A, 808. Danmarks og Grønlands Geologiske Undersøgelse Rapport 2003/54, 1–16.

Nobugai, K., Tokonami, M., Morimoto, N., 1978. A study of subsolidus relations of the Skaergaard pyroxenes by analytical electron microscopy. Contributions to Mineralogy and Petrology 67, 111–118.

Norton, D., Taylor Jr., H.P., 1979. Quantitative simulation of the hydrothermal systems of crystallizing magmas on the basis of transport theory and oxygen isotope data; an analysis of the Skaergaard Intrusion. Journal of Petrology 20, 421–486.

Osborn, E.F., 1959. Role of oxygen pressure in the crystallization and differentiation of basaltic magma. American Journal of Science 257, 609–647.

Paster, T.P., Schauwecker, D.S., Haskin, L.A., 1974. The behavior of some trace elements during solidification of the Skaergaard Layered Series. Geochimica et Cosmochimica Acta 38, 1549–1577.

Poulson, S.R., Ohmoto, H., 1990. An evaluation of the solubility of sulfide sulfur in silicate melts from experimental data and natural samples. Chemical Geology 85, 57–75.

Prendergast, M.D., 2000. Layering and Precious Metals Mineralization in the Rincón del Tigre Complex, Eastern Bolivia. Economic Geology 95, 113–130.

Ripley, E.M., Brophy, J.G., Li, C.S., 2002. Copper solubility in a basaltic melt and sulfide liquid/silicate melt partition coefficients of Cu and Fe. Geochimica et Cosmochimica Acta 66, 2791–2800.

Rudashevsky, N.S., McDonald, A.M., Cabri, L.J., Nielsen, T.F.D., Stanley, C.J., Kretser, Yu.L., Rudashevsky, V.N., 2004. Skaergaardite, PdCu, a new platinum-group intermetallic mineral from the Skaergaard Intrusion, Greenland. Mineralogical Magazine 68, 615–632.

Sato, M., Valenza, M., 1980. Oxygen fugacities of the Layered Series of the Skaergaard Intrusion, East Greenland. American Journal of Science 280A, 134–158.

Severson, M.J., Miller Jr., J.D., Peterson, D.M., Green, J.C., Hauck, S.A., 2002. Mineral potential of the Duluth Complex and related intrusions. In: Miller Jr., J.D., et al. (Eds.), Geology and Mineral Potential of the Duluth Complex and Related Rocks of Northeastern Minnesota. Minnesota Geological Survey Report of Investigations, vol. 58. University of Minnesota, Saint Paul, pp. 164–200.

Stewart, B.W., DePaolo, D.J., 1990. Isotopic studies of processes in mafic magma chambers: II. The Skaergaard Intrusion, East Greenland. Contributions to Mineralogy and Petrology 104, 125–141.

Taylor, H.P., Forester, R.W., 1979. An oxygen and hydrogen isotope study of the Skaergaard Intrusion and its country rocks: a description of a 55-M.Y. old fossil hydrothermal system. Journal of Petrology 20, 355–419.

Tegner, C., 1997. Iron in plagioclase as a monitor of the differentiation of the Skaergaard Intrusion. Contributions to Mineralogy and Petrology 128, 45–51.

Toplis, M.J., Carroll, M.R., 1996. Differentiation of ferro-basaltic magmas under conditions open and closed to oxygen: implications for the Skaergaard Intrusion and other natural systems. Journal of Petrology 37, 837–858.

Turner, P.A., 1986. The sulfide mineralogy and the behavior of S and certain trace elements in the Skaergaard Intrusion, East Greenland. Masters thesis, Dartmouth College, Hanover, New Hampshire. 79 pp.

Vincent, E.A., Crocket, J.H., 1960. Studies in the geochemistry of gold: I. The distribution of gold in rocks and minerals of the Skaergaard Intrusion, East Greenland. Geochimica et Cosmochimica Acta 18, 130–142.

Vincent, E.A., Smales, A.A., 1956. The determination of palladium and gold in igneous rocks by radioactivation analysis. Geochimica et Cosmochimica Acta 9, 154–160.

Wager, L.R., 1960. The major element variation of the Layered Series of the Skaergaard Intrusion and a re-estimation of the average composition of the Hidden Layered Series and of the successive residual magmas. Journal of Petrology 1, 364–398.

Wager, L.R., Brown, G.M., 1968. Layered Igneous Rocks. Oliver & Boyd, Edinburgh. 588 pp.

Wager, L.R., Deer, W.A., 1939. Geological investigations in East Greenland: Part III. The petrology of the Skaergaard Intrusion, Kangerdlugssuaq, East Greenland. Meddelelser om Grønland 105 (4) 352 pp.

Wager, L.R., Vincent, E.A., Smales, A.A., 1957. Sulphides in the Skaergaard Intrusion, East Greenland. Economic Geology 52, 855–903.

Wager, L.R., Vincent, E.A., Smales, A.A., 1958. The behaviour of sulphur during fractionation of basic magma. Geochimica et Cosmochimica Acta 14, 165–166.

Wood, S.A., 1987. Thermodynamic calculations of the volatility of the platinum group elements (PGE): the PGE content of fluids at magmatic temperatures. Geochimica et Cosmochimica Acta 51, 3041–3050.

Wood, S.A., 2002. The aqueous geochemistry of the platinum-group elements with applications to ore deposits. In: Cabri, L.J. (Ed.), The Geology, Geochemistry, Mineralogy, and Mineral Beneficiation of Platinum-Group Elements, vol. 54. Canadian Institute of Mining, Metallurgy, and Petroleum. CIM Special Volume, Montréal, Québec, pp. 211–250. ISBN 1-894475-27-5.